

A Musielak–Orlicz approach for modeling uncertainties in long-memory processes

Hidekazu Yoshioka^{1,*}

¹ Graduate School of Advanced Science and Technology, Japan Advanced Institute of Science and Technology, 1-1 Asahidai, Nomi, Ishikawa, Japan

* Corresponding author: yoshih@jaist.ac.jp, ORCID: 0000-0002-5293-3246

Abstract

This paper introduces a novel mathematical approach for modeling uncertainties in long-memory processes. We focus on the superposition of Ornstein–Uhlenbeck processes, the so-called supOU process, as a nominal model for complex phenomena having long memory. Uncertainties in a supOU process appear as distortions of its reversion and Lévy measures, and we propose to simultaneously assess uncertainties of these measures by using state-dependent divergence functions on Musielak–Orlicz spaces. Our approach is reduced to solving a pair of optimization problems that give upper- and lower-bounds of the cumulants of supOU processes subject to a prescribed uncertainty set. We show that classical divergence functions, such as the Kullback–Leibler one, fail to well-define these optimization problems and how this drawback can be resolved by using proper Musielak–Orlicz spaces. Moreover, we provide sufficient conditions to solve these optimization problems. We demonstrate a computational application of the proposed framework to water environmental problems where the streamflow discharge is modeled as a supOU process. This paper provides a new viewpoint for studying long-memory processes along with applications.

Keywords

Long-memory recession; supOU process; State-dependent model uncertainties; Musielak–Orlicz spaces; Applications to water environment

Statements & declarations

Acknowledgments: N.A.

Funding: This study was supported by the Japan Society for the Promotion of Science (KAKENHI No. 25K00240, 25K07931) and the Japan Science and Technology Agency (PRESTO No. JPMJPR24KE).

Conflict of Interests: The authors have no relevant financial or nonfinancial interests to disclose.

Data Availability: The data will be made available upon reasonable request to the corresponding author.

Declaration of Generative AI in Scientific Writing: Authors did not use generative AI to obtain the results of this study.

1. Introduction

1.1 Study background and motivation

Long-memory processes are stochastic processes having autocorrelation functions that decay at a polynomial speed [1] in contrast to short-memory processes, including typical Markovian processes. There are a wide variety of research fields where long-memory processes play a central role, which include but are not limited to anomalous diffusion in heterogeneous media [2], early detection of the epidemic in aquaculture [3], option pricing in finance [4], quantum dots in nanocrystals [5], electricity price forecasting [6], and gradient descent for optimization and machine learning [7].

A nominal model for long-memory phenomena is the superposition of Ornstein–Uhlenbeck processes, the so-called supOU process [8,9], which is formally a summation or integration of mutually independent Ornstein–Uhlenbeck (OU) processes having distinct reversion speeds with respect to Lévy bases¹ [10]. OU processes are representative stochastic differential equations (SDEs) whose properties have been studied extensively [e.g., 11-13], and this fact has facilitated the analysis of the supOU process. Despite its simplicity, supOU processes have rich mathematical structures due to their diverse long-memory and fluctuation properties encoded in Lévy bases. To date, supOU processes have been applied to volatilities in economics [14] and environmental [15] and ecological problems [16]. Their memory and spectral characteristics have been investigated in Kovtun et al. [17], and growth and extremes have been investigated in Grahovac and Kevei [18] and Moser and Stelzer [19]. Leonenko and Pepelyshev [20] discussed theoretical and computational methodologies to efficiently simulate jump-driven supOU processes with prescribed probability density functions (PDFs). Long-memory processes related to supOU processes, such as the Volterra and Trawl processes [21] as well as superpositions of nonlinear SDEs [22,23], have also been theoretically studied.

This paper focuses on jump-driven supOU processes because they frequently appear in applied problems where the nonnegativity of solutions is necessary, such as the case for volatility and streamflow discharge [14-16] and environmental problems [23], and because the framework of uncertainty modeling in this paper straightforwardly applies to cases with diffusion. Behavior and mathematical properties of a jump-driven supOU process are determined by the two measures: the reversion measure to distribute reversion rates and the Lévy measure that governs the size and frequency of jumps. The singularity of a reversion measure determine the memory strength, namely, the decay of the autocorrelation function, of a supOU process, while the Lévy measure quantifies the moments and path regularities of this process. Therefore, perturbing these measures results in qualitatively and/or quantitatively different supOU processes in theory and different statistical predictions in application. Because the estimation of reversion and Lévy measures amounts to the identification of a supOU process, quantifying the relationship between uncertainties (i.e., modeling errors) introduced in these measures and the resulting model is important in both theory and application.

¹ Lévy bases are space-time generalization of Lévy processes and are seen as high-dimensional Poisson random measures for pure-jump cases [9].

Uncertainties in stochastic models may come from data and assumptions. First, available data in an applied problem would contain measurement errors due to technical restrictions [24,25]. Second, the quantity of data, such as the length of time series is usually restricted [26,27]. Third, the assumed model may deviate from the ground truth due to assuming improper functional forms of its [28,29]. Finally, even if the data are complete in quality and quantity, the identification procedure may become a source error. In any case, quantifying and, if possible, predicting the possible range of uncertainties is a key step toward operating a misspecified stochastic process model.

Thus far, modeling uncertainties in reversion and Lévy measures have been carried out separately, assuming that one of them is correct [30,31]; however, this assumption is too strong because both measures would be estimated based on a common time series dataset for the target phenomenon. This means that there is a gap between the theory and application for modeling uncertainties in supOU processes, motivating us to develop a unified mathematical framework that can simultaneously address uncertainties contained in reversion and Lévy measures.

1.2 Aim and contribution

The aims of this paper are to formulate and analyze a unified framework for dealing with uncertainties in jump-driven supOU processes and present its applications, with which we will be able to abandon the assumption that uncertainties are concentrated solely on either a reversion measure or a Lévy measure. An important advantage of the proposed mathematical framework is its capability to evaluate the influences of uncertainties on the statistics of supOU processes, which are non-Markovian processes, without resorting to Monte Carlo simulations.

We focus on the state-dependent uncertainty assessment approach recently proposed in Strati [32], whose primary direction was insurance, while their mathematical tools, especially Musielak–Orlicz spaces (Chapter 3 in Chlebicka et al. [33]), carry over to any measures having finite masses; reversion and Lévy measures of supOU processes are not exception. We exploit the useful features of supOU processes such that its cumulants and autocorrelations are given by certain (non)polynomial moments of the two measures, which provide the relationship to clearly show how uncertainties in these measures propagate to statistics of supOU processes.

A method meaningful in application to estimate impacts of uncertainties on a statistic is to evaluate the size of uncertainties by using a divergence, also called statistical divergence, which quantifies the difference between two different stochastic models [34]. This methodology was reviewed in Ben-Tal and Teboulle [35] and was later systematized in Fröhlich and Williamson [36] based on Orlicz spaces, which are function spaces of random variables that have a certain strength of singularity, such as nonpolynomial integrability (Chapter 13 in Rubshtein et al. [37]). Finding a proper Orlicz space to which the target random variable belongs allows for the construction of divergences that are well-defined and computable. We focus on the state-dependence in divergences, but qualitatively similar approaches would apply to related risk indices such as the robust return risk measures [38,39] and Orlicz premia [40,41], where the well-posedness of optimization problems is determined by Orlicz spaces.

The limitation of the approach based on classical Orlicz spaces is that it cannot deal with state-dependent divergences. Here, the state-dependence means the situation where a parameter or a coefficient of divergence depends on the randomness coming from other than the target random variable. For the case of supOU processes, this corresponds to the situation where uncertainties affect both reversion and Lévy measures, and that accounting for the state-dependence is essential due to their cumulant forms. Strati [32] proposed using Musielak–Orlicz spaces instead of classical Orlicz spaces, with which the state-dependence can be naturally formulated. We employ this recently developed theory to formulate both upper and lower bounds of cumulants of supOU processes, with which we can estimate the cumulants subject to uncertainties by finding proper solutions to optimization problems formulated with Musielak–Orlicz spaces. We show that the classical divergences, such as the Kullback–Leibler (KL) divergence, fail to well-define these optimization problems and that allowing for its state-dependence resolves this issue. We also discuss what state-dependence is allowed for the alpha divergence: a popular generalization of the KL one [e.g., 42,43].

In our framework, the supOU process under uncertainties, i.e., the distorted supOU process, is different from the classical ones because reversion and Lévy measures turn out to be interdependent in the former but not in the latter. This implies that we need to check the integrability condition to verify the well-posedness of ambit fields (Proposition 39 in Barndorff-Nielsen et al. [21]), and moreover, its connection to the solvability of our optimization problems should be clarified. We show how the conditions for well-posedness are linked between the distorted supOU process and our optimization problems by focusing on state-dependence.

We also contribute to computational aspects of modeling uncertainties in supOU processes. Our optimization problems to evaluate the cumulants subject to uncertainties can be computationally solved by a gradient descent method with momentum along with a quantization method to discretize expectations. This method provides not only the solution but also optimal Lagrangian multipliers (Chapter 5.6.2 in Boyd and Vandenberghe [44]), which are sensitivities about constraints about the uncertainty set and hence are useful for deeper understanding the influences of uncertainties in the proposed framework.

Finally, we present demonstrative applications of the proposed mathematical framework to supOU processes fitted against real streamflow discharge data. Indeed, streamflow discharge as a physical quantity characterizing the water quantity in river environments exhibits polynomial and hence slow recessions after flood events [45-47], requiring the use of a long-memory process for its mathematical modeling. Moreover, each flood event can be considered a jump event [48-50]. We analyze how the reversion and Lévy measures are distorted subject to uncertainties and how the resulting supOU processes behave in both statistics and threshold dynamics. Consequently, this paper contributes to formulation through the application of uncertainty modeling for long-memory processes by focusing on supOU processes.

1.3 Organization of this paper

Section 2 introduces the supOU process studied in this paper. **Section 3** presents our mathematical framework for modeling uncertainties in supOU processes and theoretically analyzes a pair of optimization

problems. **Section 4** applies our mathematical framework to real data. **Section 5** summarizes this paper and presents perspectives on our study. **Appendix** presents proofs of propositions and supplementary results.

2. supOU process

2.1 Formulation

In this subsection, we formulate a supOU process whose Lévy base admits a nonclassical structure where the influences of reversion and jump are not decomposable. We work on a filtered complete probability space as usual in stochastic calculus for continuous-time processes [e.g., 14].

Time t is a real independent variable. As a supOU process, we consider the following continuous-time stochastic process $X = (X_t)_{t \in \mathbb{R}}$:

$$X_t = \int_{r=0}^{r=+\infty} \int_{z=0}^{z=+\infty} \int_{s=-\infty}^{s=+\infty} \underbrace{z}_{\text{Jump size}} \underbrace{e^{-r(t-s)} \mathbb{I}(s < t)}_{\text{Reversion}} \underbrace{N_\phi(dr, dz, ds)}_{\text{Randomness}}, \quad t \in \mathbb{R}, \quad (1)$$

where $\mathbb{I}(s < t)$ is the indicator function such that $\mathbb{I}(s < t) = 1$ if $s < t$ and $\mathbb{I}(s < t) = 0$ otherwise, $r > 0$ represents distributed reversion speeds, $z > 0$ represents distributed jump sizes, N represents a Poisson random measure on $(0, +\infty) \times (0, +\infty) \times \mathbb{R}$ with the compensated measure $\phi(r, z) \pi(dr) \nu(dz) ds$ with π being a probability measure of a positive random variable, $\nu(dz)$ is a Lévy measure satisfying the integrability condition $\int_0^{+\infty} z \nu(dz) < +\infty$ (necessary for the existence of average of (1) when $\phi \equiv 1$), and ϕ is a nonnegative function on $(0, +\infty) \times (0, +\infty)$. Note that $\nu(dz)$ needs not be a probability measure but $\pi(dr)$ does.

The supOU process (1) is non-Markovian because the right-hand side of (1) can be understood as an aggregation of mutually independent background OU processes [8]. More specifically, the expectation of the current value X_t conditioned on the past value X_s is different from that on all the background OU processes at time s ; the information by the former is smaller than the latter, which gives the non-Markovian nature of the supOU process.

Remark 1 We recover the classical supOU process with $\phi \equiv 1$ [8].

Remark 2 In **Section 3**, we encounter $\phi = z^{m_1} r^{-m_2}$ and $\phi = \exp(m_3 z^{m_1} r^{-m_2})$ with $m_1, m_2 > 0$, $m_3 \in \mathbb{R}$ up to multiplication constants.

In classical supOU processes ($\phi \equiv 1$), the compensated measure of the Poisson random measure has a separable structure between reversion and Lévy measures, while (1) does not due to the appearance of the bivariate function ϕ . Physically, this ϕ implies an interdependence between reversion and jump, e.g., a model where the distributions of jump size and frequency depend on reversion rate or the distribution of reversion speeds depends on jump size. In our context, nonconstant ϕ cases arise due to assuming

modeling errors that simultaneously affect reversion and jumps of supOU processes. More specifically, the supOU process (1) arises as a distorted model based on the assumption that a classical supOU process is identified as a model estimated from data, while in reality, there is a possibility that influences of reversion and jump are not decomposable.

2.2 Mathematical structure

We need to ensure under what condition the right-hand side of (1) exists because we are not aware of literature that explicitly deals with supOU processes of this form. We exploit the integrability condition for ambit fields and adapt it to (1) (Proposition 39 in Barndorff-Nielsen et al. [21]).

Proposition 1

The process X in (1) exists and stationary if

$$\int_{r=0}^{r=+\infty} \int_{z=0}^{z=+\infty} \int_{s=-\infty}^{s=+\infty} \min\{1, z^2 e^{-2rs}\} \phi(r, z) \pi(dr) \nu(dz) ds < +\infty. \quad (2)$$

Moreover, the characteristic function $\mathbb{E}[e^{uX_t}]$ ($t \in \mathbb{R}$) is independent of t and is given by (i represents the imaginary unit: $i^2 = -1$)

$$\ln \mathbb{E}[e^{uX_t}] = \int_{r=0}^{r=+\infty} \int_{z=0}^{z=+\infty} \int_{s=-\infty}^{s=+\infty} (\exp(iue^{-rs}z) - 1) \phi(r, z) \pi(dr) \nu(dz) ds, \quad u \in \mathbb{R}. \quad (3)$$

For the classical case ($\phi \equiv 1$), the integrability condition (2) is satisfied if the inverse moment of π exists:

$$\int_0^{+\infty} r^{-1} \pi(dr) < +\infty. \quad (4)$$

Under (4), the classical supOU process is stationary and infinitely divisible (Theorem 3.1 in Barndorff-Nielsen and Stelzer [9]). Another key assumption that we employ is about densities:

Assumption 2 Measures π and ν admit positive densities.

This is a technical assumption to ensure the existence of solutions to our optimization problems but is satisfied by many examples in the literature [e.g., 20,30]. We assume that **Assumptions 1 and 2** hold true in the rest of this paper.

For later use, we set the following integrability conditions:

$$(\mathbf{I}_k) \quad I_k = \frac{1}{k} \int_{r=0}^{r=+\infty} \int_{z=0}^{z=+\infty} \frac{\phi(r, z) z^k}{r} \pi(dr) \nu(dz) < +\infty, \quad k \in \mathbb{N}. \quad (5)$$

The condition (2) is satisfied if **(I₂)** is, because

$$\begin{aligned}
& \int_{r=0}^{r=+\infty} \int_{z=0}^{z=+\infty} \int_{s=-\infty}^{s=+\infty} \min\{1, z^2 e^{-2rs}\} \phi(r, z) \pi(dr) \nu(dz) ds \\
& \leq \int_{r=0}^{r=+\infty} \int_{z=0}^{z=+\infty} \int_{s=-\infty}^{s=+\infty} z^2 e^{-2rs} \phi(r, z) \pi(dr) \nu(dz) ds \\
& = \int_{r=0}^{r=+\infty} \int_{z=0}^{z=+\infty} \int_{s=-\infty}^{s=+\infty} \frac{\phi(r, z) z^2}{2r} \pi(dr) \nu(dz) ds.
\end{aligned} \tag{6}$$

The cumulants and autocorrelation function of (1) are derived explicitly. For example, because the left-hand side of (3) represents a cumulant generating function, we have

$$\text{Cum}_k = I_k \quad \text{under } (\mathbf{I}_k), \quad k \in \mathbb{N} \tag{7}$$

and

$$\text{ACF}(h) = \frac{\mathbb{E}[(X_t - \mathbb{E}[X_t])(X_{t+h} - \mathbb{E}[X_{t+h}])]}{\text{Cum}_2} = I_2^{-1} \int_{r=0}^{r=+\infty} \int_{z=0}^{z=+\infty} \frac{\phi(r, z) z^2}{2r} e^{-rh} \pi(dr) \nu(dz) \quad \text{under } (\mathbf{I}_2), \tag{8}$$

where Cum_k represents the k th order cumulant and $\text{ACF}(h)$ is the autocorrelation function with lag $h \geq 0$. Particularly, the cases $k=1, 2, 3$ represent average, variance, and nonnormalized skewness, respectively.

By a Tauberian argument [51], we can evaluate the tail of the autocorrelation function according to singularities of ϕ and π when h is large, as shown in the next proposition. The asymptotic condition (9) means that the supOU process (1), as for the classical case, has a long-memory property if the integrand in (8) has a certain range of singularities near $r=0$. The difference is that the singularity depends on both ϕ and π in the present case.

Proposition 2

Assume the condition (\mathbf{I}_2) and that π admits a density p . If the following asymptotic estimate holds true for some constant $A > 1$:

$$\frac{\phi(r, z) p(r)}{r} \sim O(r^{A-2}) \quad \text{with respect to } 0 < r \ll 1 \text{ for all } z > 0, \tag{9}$$

then

$$\text{ACF}(h) = O(h^{-(A-1)}) \quad \text{for } h \gg 1. \tag{10}$$

Particularly, this proposition implies that the tail behavior of the autocorrelation function is the same for all ϕ that are bounded near $r=0$. Note that the parameter A serves as the Hurst index if $A \in (1, 2]$.

Remark 3 According to (5), (7), (8), and **Propositions 1-2**, the condition (\mathbf{I}_2) is sufficient for stationarity of the supOU process (1) with bounded variance and possibly long-memory autocorrelation function.

3. The Musielak–Orlicz framework

3.1 Problem setting

We consider a situation where we have identified a classical supOU process (the process (1) with $\phi \equiv 1$, called the benchmark model in the sequel) from a limited dataset, but the true model corresponds to $\phi \neq 1$ (distorted model). In this case, we have estimations of the reversion measure π and Lévy measure ν but are not necessarily correct, and the difference between the benchmark and distorted models is evaluated by ϕ .

3.1.1 Generalized alpha divergence

In this paper, the difference between the benchmark and distorted models is evaluated through the generalized alpha divergence $\mathbb{D}(\phi)$: for positive and continuous functions w, α on $(0, +\infty) \times (0, +\infty)$,

$$\mathbb{D}(\phi) = \int_{r=0}^{r=+\infty} \int_{z=0}^{z=+\infty} \underbrace{\Phi \left(\underbrace{w(r, z)}_{\text{Weighting}}, \underbrace{\alpha(r, z)}_{\text{Shape}}, \underbrace{\phi(r, z)}_{\text{Uncertainty}} \right)}_{\text{Divergence function}} \pi(dr) \nu(dz) \quad (11)$$

with Φ given by

$$\Phi(w_0, \alpha_0, \phi_0) = \begin{cases} w_0 \frac{(\phi_0)^{\alpha_0} - \alpha_0 (\phi_0 - 1) - 1}{\alpha_0 (\alpha_0 - 1)} & (\alpha_0 \neq 1) \\ w_0 (\phi_0 \ln \phi_0 - \phi_0 + 1) & (\alpha_0 = 1) \end{cases}, \quad w_0, \alpha_0, \phi_0 \geq 0. \quad (12)$$

We set $\Phi(w_0, \alpha_0, \phi_0) = +\infty$ for $\phi_0 < 0$, which extends the domain of Φ to $\phi_0 \in \mathbb{R}$ without losing convexity. This extension plays a role in the derivation of the dual representations of our optimization problems. The divergence $\mathbb{D}(\phi)$ is able to evaluate the difference between benchmark and distorted models; $\Phi = 0$ if there is no uncertainty ($\phi \equiv 1$), and is positive otherwise.

With (11), we generalize the classical alpha divergence (e.g., Eq. (1) in Póczos and Schneider [43]) in three ways. First, we extend the domain of divergence from a PDF to a positive measurable function because of our modeling assumption that the function ϕ in (1) needs not be a PDF. Second, we assume that the parameter α depends on r, z , while the classical alpha divergence assumes α as a positive constant, which offers a more flexible framework for modeling uncertainties. As shown in (12), the generalized alpha divergence is reduced to the classical KL one when $\alpha \equiv 1$ and $w \equiv 1$. Finally, the function w serving as a weighting factor further increases the flexibility in modeling uncertainties, but its true value is revealed with the modified KL divergence function ($\alpha \equiv 1$ but $w \neq 1$) with which our optimization problems become well-defined; the classical KL case never succeeds for the supOU process.

We summarize the properties of Φ in **Lemma 1**, which follow from direct calculations:

Lemma 1

For each $w_0, \alpha_0 > 0$, $\Phi(w_0, \alpha_0, \phi_0)$ as a function of $\phi_0 \geq 0$ is continuous, convex, nonnegative, and globally minimized at $\phi_0 = 1$ with the minimum value $\Phi(w_0, \alpha_0, 1) = 0$. Moreover,

$$\lim_{\phi_0 \rightarrow +0} \Phi(w_0, \alpha_0, \phi_0) < +\infty, \quad \lim_{\phi_0 \rightarrow +\infty} \Phi(w_0, \alpha_0, \phi_0) = +\infty \quad \text{and} \quad \lim_{\phi_0 \rightarrow +\infty} \frac{\Phi(w_0, \alpha_0, \phi_0)}{\phi_0} = +\infty \quad \text{when} \quad \alpha_0 \geq 1.$$

3.1.2 Optimization problems

We consider the following pair of optimization problems where we emphasize the dependence of the cumulant $\text{Cum}_k = I_k$ on ϕ (for the definition of I_k , recall (5)): for each fixed $k, m = 0, 1, 2, \dots$ and $\varepsilon > 0$,

Upper-bound case Find $\bar{I}_{k,m} = \sup_{\phi \in \mathfrak{A}_{m,\varepsilon}} \text{Cum}_k(\phi) = \sup_{\phi \in \mathfrak{A}_{m,\varepsilon}} I_k(\phi)$ (13)

Lower-bound case Find $\underline{I}_{k,m} = \inf_{\phi \in \mathfrak{A}_{m,\varepsilon}} \text{Cum}_k(\phi) = \inf_{\phi \in \mathfrak{A}_{m,\varepsilon}} I_k(\phi)$ (14)

Here, $\mathfrak{A}_{m,\varepsilon}$ is the following admissible set of measurable functions:

$$\text{Find } \mathfrak{A}_{m,\varepsilon} = \left\{ \phi: (0, +\infty)^2 \rightarrow [0, +\infty) \mid I_m(\phi) = c_m, \mathbb{D}(\phi) \leq \varepsilon \right\}, \tag{15}$$

where $c_m > 0$ is the m th-order cumulant in the benchmark case:

$$c_m = \frac{1}{m} \int_{r=0}^{r=+\infty} \int_{z=0}^{z=+\infty} \frac{z^m}{r} \pi(dr) \nu(dz). \tag{16}$$

The constraint “ $I_m(\phi) = c_m$ ” is omitted when $m = 0$ because of (4). The pair (13)-(14) gives upper and lower bounds of the cumulant subject to the uncertainty size ε evaluated in terms of the divergence $\mathbb{D}(\phi)$. By definitions of $\bar{I}_{k,m}, \underline{I}_{k,m}$, we have

$$0 \leq \underline{I}_{k,m} \leq \text{Cum}_k(1) \leq \bar{I}_{k,m}, \tag{17}$$

showing that $\bar{I}_{k,m}, \underline{I}_{k,m}$ sandwich the cumulant $\text{Cum}_k(1)$ of the benchmark case. The goal of the optimization problems is to find the maximizing/minimizing $\phi = \phi^*$, which correspond to the worst-case uncertainties in the supOU process given an uncertainty size.

Remark 4 Because the estimation of a cumulant would be more sensitive to data for higher m as discussed above, it is reasonable to assume $k > m$. In **Section 4**, we focus on the cases $(k, m) = (1, 0)$ (average is uncertain) and $(k, m) = (2, 1)$ (variance is uncertain and average is more reliable).

Remark 5 The relationship (17) shows a qualitative difference between $\bar{I}_{k,m}, \underline{I}_{k,m}$ because the latter is not bounded from above, while the former is bounded from below by 0 and from above by $\text{Cum}_k(1)$. The **Upper-bound case** is therefore more delicate.

3.2 Mathematical analysis

We study the existence and computability of optimizing ϕ in (13)-(14). In the sequel, we assume $k > m \geq 1$ because the results on the case $m = 0$ follow by suitably omitting the constraint in (15) and

Remark 4. We first analyze the **Upper-bound case** that is more delicate, and then the **Lower-bound case**.

3.2.1 Upper-bound case

We need to carefully formulate the divergence because otherwise $\bar{I}_{k,m} = +\infty$. We analyze the **Upper-bound case** by focusing on when this unboundedness issue occurs with the help of Musielak–Orlicz spaces. For this purpose, we set the following function that is convex and increasing for $\phi_0 \geq 0$ by **Lemma 1**:

$$\bar{\Phi}(w_0, \alpha_0, \phi_0) = \begin{cases} 0 & (0 \leq \phi_0 \leq 1) \\ \Phi(w_0, \alpha_0, \phi_0) & (\phi_0 > 1) \end{cases}, \quad w_0, \alpha_0 > 0. \quad (18)$$

We set the convex conjugate Ψ of Φ with respect to the third argument: for each $w_0, \alpha_0 > 0$,

$$\Psi(w_0, \alpha_0, \psi_0) = \sup_{\phi_0 > 0} \{ \psi_0 \phi_0 - \Phi(w_0, \alpha_0, \phi_0) \}, \quad \psi_0 \in \mathbb{R}. \quad (19)$$

Similarly, the convex conjugate of $\bar{\Phi}$ is denoted as $\bar{\Psi}$, which is given by (19) with the replacement $\Phi \Rightarrow \bar{\Phi}$. We have **Lemma 2** by direct calculations in (19) (see also Proposition 3.11 in Fröhlich and Williamson [36]):

Lemma 2

For each $w_0, \alpha_0 > 0$ and $\psi_0 \in \mathbb{R}$,

$$\Psi(w_0, \alpha_0, \psi_0) = \frac{w_0}{\alpha_0} \left\{ \max \left\{ 0, 1 + (\alpha_0 - 1) \frac{\psi_0}{w_0} \right\}^{\frac{\alpha_0}{\alpha_0 - 1}} - 1 \right\} \quad (20)$$

if $\alpha_0 \neq 1$ and

$$\Psi(w_0, \alpha_0, \psi_0) = w_0 \left(\exp \left(\frac{\psi_0}{w_0} \right) - 1 \right) \quad (21)$$

if $\alpha_0 = 1$, where the right-hand side of (20) is understood to be $+\infty$ if $0 < \alpha_0 < 1$ and $1 + (\alpha_0 - 1)\psi_0 \leq 0$, and similarly,

$$\frac{\partial \Psi(w_0, \alpha_0, \psi_0)}{\partial \psi_0} = \begin{cases} \max \left\{ 0, 1 + (\alpha_0 - 1) \frac{\psi_0}{w_0} \right\}^{\frac{1}{\alpha_0 - 1}} & (\alpha_0 \neq 1) \\ \exp \left(\frac{\psi_0}{w_0} \right) & (\alpha_0 = 1) \end{cases}, \quad (22)$$

where the right-hand side of (22) is set to $+\infty$ if $0 < \alpha_0 < 1$ and $1 + (\alpha_0 - 1)\psi_0 \leq 0$. This Ψ is nondecreasing and convex as a function of $\psi_0 \in \mathbb{R}$. Moreover, $\bar{\Psi} = \Psi$ for $\psi_0 \geq 0$. Finally,

$$-\frac{w_0}{\alpha_0} \leq \Psi(w_0, \alpha_0, \psi_0) \leq \bar{\Psi}(w_0, \alpha_0, \psi_0), \quad \psi_0 \in \mathbb{R}. \quad (23)$$

The product measure $\pi \nu$ is not necessarily a probability measure on $(0, +\infty)^2$, but we can construct a probability measure on the basis of the constraint $I_m(\phi) = c_m$; we can rewrite it as

$$\int_{r=0}^{r=+\infty} \int_{z=0}^{z=+\infty} \phi(r, z) \underbrace{\frac{z^m}{c_m m r} \pi(dr) \nu(dz)}_{p_m(dr, dz)} = 1 \quad (24)$$

with

$$p_m(dr, dz) = \left(\int_{r=0}^{r=+\infty} \int_{z=0}^{z=+\infty} \frac{z^m}{m r} \pi(dr) \nu(dz) \right)^{-1} \frac{z^m}{m r} \pi(dr) \nu(dz), \quad r, z > 0 \quad (25)$$

being a probability measure on $(0, +\infty)^2$ by (16). Then, ϕ is seen as a Radon-Nikodym derivative that satisfies $\mathbb{E}_m[\phi] = 1$, where \mathbb{E}_m represents the expectation based on p_m . In the sequel, we symbolically write an integration with respect to p_m as an expectation \mathbb{E}_m in a suitable probability space, e.g., $\mathbb{E}_m[\phi]$ can be identified as the left-hand side of (24).

With p_m , we can reformulate the optimization problem (13) as follows:

$$\text{Find } \bar{I}_{k,m} = \frac{m c_m}{k} \sup_{\phi \in \mathfrak{A}_{m,\varepsilon}} \mathbb{E}_m \left[z^{k-m} \phi(r, z) \right] \quad (26)$$

with $\mathfrak{A}_{m,\varepsilon}$ reformulated as a

$$\mathfrak{A}_{m,\varepsilon} = \left\{ \phi: (0, +\infty)^2 \rightarrow [0, +\infty) \mid \mathbb{E}_m[\phi] = 1, \mathbb{D}'(\phi) \leq \frac{\varepsilon}{m c_m} \right\}, \quad (27)$$

where

$$\begin{aligned} \mathbb{D}'(\phi) &= \int_{r=0}^{r=+\infty} \int_{z=0}^{z=+\infty} \frac{r}{z^m} \Phi(w(r, z), \alpha(r, z), \phi(r, z)) p_m(dr, dz) \\ &= \int_{r=0}^{r=+\infty} \int_{z=0}^{z=+\infty} \Phi\left(\frac{r}{z^m} w(r, z), \alpha(r, z), \phi(r, z)\right) p_m(dr, dz) \\ &= \mathbb{E}_m[\Phi(w', \alpha, \phi)]. \end{aligned} \quad (28)$$

We have omitted the arguments of $\bar{\Phi}$ in (28). In (28), we set $w' = rz^{-m}w$, which is an inhomogeneous and hence state-dependent function even when w is a constant. Now, the optimization problem has been reformulated as a maximization problem to determine a maximizing Radon-Nikodym derivative. The price to pay is that the weight w' may be more complex than w .

By **Lemma 1** and the reformulation above, we can associate a Musielak–Orlicz space, which is a Banach space (Section 2 in Strati [32]), to the function $\bar{\Phi}$.

Definition 1

The Musielak–Orlicz space $L_{\bar{\Phi}}$ is a collection of all real random variables ϕ on $(0, +\infty)^2$ such that

$$\mathbb{E}_m \left[\bar{\Phi} \left(w', \alpha, \frac{|\phi|}{c} \right) \right] < +\infty \quad (29)$$

for some constant $c > 0$, and the space $L_{\bar{\Phi}}$ is equipped with the norm

$$\|\phi\|_{\bar{\Phi}} = \inf \left\{ c > 0 \mid \mathbb{E}_m \left[\bar{\Phi} \left(w', \alpha, \frac{|\phi|}{c} \right) \right] \leq 1 \right\}. \quad (30)$$

We associate another Musielak–Orlicz space $L_{\bar{\Psi}}$ to $\bar{\Psi}$, which is defined with the formal replacement $\bar{\Phi} \Rightarrow \bar{\Psi}$ in **Definition 1**. The Musielak–Orlicz space $L_{\bar{\Phi}}$ is reduced to a classical Orlicz space if w and α are constant functions.

We consider the following standard structural condition about $\bar{\Phi}$, the so-called (uniform) Δ_2 condition, which ensures the reflexivity of $L_{\bar{\Phi}}$ with its dual $L_{\bar{\Psi}}$ (e.g., Section 2 in Strat [32]).

Assumption 3 There exists a constant $K > 0$ such that

$$\bar{\Phi}(w_0, \alpha_0, 2\phi_0) \leq K \bar{\Phi}(w_0, \alpha_0, \phi_0) \text{ for all } w_0, \alpha_0, \phi_0 > 0. \quad (31)$$

The next proposition gives an existence result and a dual reformulation of the **Upper-bound case**, which is computationally accessible. Musielak–Orlicz spaces play a role here.

Proposition 3

Assume $z^{k-m} \in L_{\bar{\Psi}}$ and **Assumption 3**. The optimization problem (13) is reformulated as

$$\begin{aligned} \bar{I}_{k,m} &= \frac{mc_m}{k} \inf_{\mu \in \mathbb{R}, \tau > 0} \left\{ \frac{\varepsilon}{mc_m} \tau + \mu + \tau \mathbb{E}_m \left[\Psi \left(w'(r, z), \alpha(r, z), \frac{z^{k-m} - \mu}{\tau} \right) \right] \right\} \\ &= \left(\frac{mc_m}{k} \inf_{\mu \in \mathbb{R}, \tau > 0} F(\tau, \mu) \right) \end{aligned} \quad (32)$$

with the infimum being attained at an interior point $(\hat{\tau}, \hat{\mu}) \in (0, +\infty) \times [0, +\infty)$. Moreover, an optimal $\phi = \phi^*$ is given by

$$\phi^*(r, z) = \frac{\partial \Psi}{\partial \psi} \left(w'(r, z), \alpha(r, z), \frac{z^{k-m} - \hat{\mu}}{\hat{\tau}} \right), \quad (33)$$

and it satisfies the condition **(I_k)**. The couple $(\hat{\tau}, \hat{\mu})$ solves the equations

$$\frac{\partial F(\tau, \mu)}{\partial \tau} = 0 \quad \text{and} \quad \frac{\partial F(\tau, \mu)}{\partial \mu} = 0. \quad (34)$$

Here, the Δ_2 condition (**Assumption 3**) ensures the existence of a minimizer of (32). This condition is satisfied for (12) with strictly bounded α , but the condition $z^{k-m} \in L_{\bar{\Psi}}$ may fail if $\alpha(r, z) < 1$ for some (r, z) because of (20) unless w is chosen properly (see **Section 3.2.4**). Note also that the assumption $z^{k-m} \in L_{\bar{\Psi}}$ can be checked once a divergence is given before solving the optimization problem, while the condition **(I_k)** cannot be because it uses the optimizer ϕ^* , which is unknown. However, if $z^{k-m} \in L_{\bar{\Psi}}$, then the condition **(I_k)** with ϕ^* holds true as stated in the proposition, and this is the place where Musielak–Orlicz spaces determine the existence of the cumulants of the supOU process (1).

Remark 6 Inspecting **Proof of Proposition 3** shows that this proposition holds true if Φ is replaced by another function that satisfies certain properties (nonnegativity, convexity, minimized at $\phi_0 = 1$, and $\Phi(\cdot, \cdot, +\infty) = +\infty$) in **Lemma 1**, the Δ_2 condition (**Assumption 3**), and the continuous differentiability of $\Psi(\cdot, \cdot, \psi_0)$ for all $\psi_0 \in \mathbb{R}$. One can apply the arguments in Proof of Proposition 5.5 and Proof of Theorem 6.5 in Dommel and Pichler [52].

3.2.2 Lower-bound case

We have

$$\underline{I}_{k,m} = \inf_{\phi \in \mathfrak{A}_{m,\varepsilon}} I_k(\phi) = \inf_{\phi \in \mathfrak{A}_{m,\varepsilon}} \{-I_k(-\phi)\} = - \sup_{\phi \in \mathfrak{A}_{m,\varepsilon}} I_k(-\phi). \quad (35)$$

This is essentially a maximization problem analogous to the **Upper-bound case**, and we have the following proposition.

Proposition 4

Assume $z^{k-m} \in L_{\bar{\Psi}}$ and **Assumption 3**. The optimization problem (14) is reformulated as

$$L_{k,m} = -\frac{mc_m}{k} \inf_{\mu \in \mathbb{R}, \tau > 0} \left\{ \frac{\varepsilon}{mc_m} \tau + \mu + \tau \mathbb{E}_m \left[\Psi \left(w'(r, z), \alpha(r, z), \frac{-z^{k-m} - \mu}{\tau} \right) \right] \right\} \quad (36)$$

$$\left(= -\frac{mc_m}{k} \inf_{\mu \in \mathbb{R}, \tau > 0} G(\tau, \mu) \right)$$

with the infimum attained at an interior point $(\hat{\tau}, \hat{\mu}) \in (0, +\infty) \times (-\infty, 0]$. Moreover, an optimal $\phi = \phi^*$ is given by

$$\phi^*(r, z) = \frac{\partial \Psi}{\partial \psi} \left(w'(r, z), \alpha(r, z), \frac{-z^{k-m} - \hat{\mu}}{\hat{\tau}} \right), \quad (37)$$

and it satisfies the condition (\mathbf{I}_k) . The couple $(\hat{\tau}, \hat{\mu})$ solves the equations

$$\frac{\partial G(\tau, \mu)}{\partial \tau} = 0 \quad \text{and} \quad \frac{\partial G(\tau, \mu)}{\partial \mu} = 0. \quad (38)$$

3.2.3 Ordering Musielak–Orlicz spaces

There is an ordering property among Musielak–Orlicz spaces, as shown in the next proposition, which is a state-dependent extension of the result for classical Orlicz spaces (Proposition 4 in Yoshioka and Yoshioka [30]). Here, the Musielak–Orlicz space associated with $\bar{\Phi}(w', \alpha, \cdot)$ is denoted as $L_{\bar{\Phi}(w', \alpha, \cdot)}$ with the associated norm $\|\cdot\|_{\bar{\Phi}(w', \alpha, \cdot)}$.

Proposition 5

If $\bar{\Phi}(w'_1, \alpha_1, \cdot) \leq \bar{\Phi}(w'_2, \alpha_2, \cdot)$ then $L_{\bar{\Phi}(w'_2, \alpha_2, \cdot)} \subset L_{\bar{\Phi}(w'_1, \alpha_1, \cdot)}$. Moreover, if $\phi \in L_{\bar{\Phi}(w'_2, \alpha_2, \cdot)}$, then $\|\phi\|_{\bar{\Phi}(w'_2, \alpha_2, \cdot)} \geq \|\phi\|_{\bar{\Phi}(w'_1, \alpha_1, \cdot)}$.

The statement of this proposition is simple but intuitive. Indeed, in the context of our optimization problems, a smaller Musielak–Orlicz space is more pessimistic about uncertainties because it corresponds to a larger divergence.

3.2.4 Specific setting

We discuss the implications of **Propositions 3-4** focusing on a specific setting that is encountered in applied problems. Here, we use the measures π and ν rather than p_m because the latter has been introduced for technical reasons. Similarly, we use w rather than w' . We study when the condition (\mathbf{I}_k) is satisfied with the optimal $\phi = \phi^*$ and then how the autocorrelation function would behave. We focus mainly on the **Upper bound case** in this subsection.

Because we are interested in long-memory phenomena in supOU processes, we assume the following gamma distribution for the reversion measure π , which is a nominal model for reversion rates [e.g., 8,9,30]:

$$\pi(dr) = c_\pi r^{A-1} e^{-\frac{r}{B}} dr, \quad r > 0 \quad (39)$$

with the shape parameter $A > 1$, scale parameter $B > 0$, and normalization constant $c_\pi > 0$. For the Lévy measure ν , we assume the following tempered-stable model, which is a common model for describing jumps [e.g., 20,53,54]:

$$\nu(dz) = c_\nu \frac{e^{-pz}}{z^{q+1}} dz, \quad z > 0 \quad (40)$$

with the shape parameter $q < 1$, tilting parameter $p > 0$, and intensity parameter $c_\nu > 0$. Under the present setting, the condition (\mathbf{I}_k) becomes

$$I_k = \frac{c_\pi c_\nu}{k} \int_{r=0}^{r=+\infty} \int_{z=0}^{z=+\infty} \phi(r, z) r^{A-2} z^{k-q-1} e^{-\frac{r}{B} - pz} dr < +\infty, \quad k \in \mathbb{N}. \quad (41)$$

This implies that (\mathbf{I}_m) is satisfied if (\mathbf{I}_k) is ($m < k$). We assume $m < k$ in the rest of this subsection.

Now, we investigate the link between the singularity of the measures π, ν and the function Φ .

First, we assume that $\alpha(\cdot, \cdot) > 1$. By direct calculations,

$$\phi^*(r, z) = \max \left\{ 0, 1 + \frac{\alpha(r, z) - 1}{w'(r, z)} \frac{z^{k-m} - \hat{\mu}}{\hat{t}} \right\}^{\frac{1}{\alpha(r, z) - 1}} = \max \left\{ 0, 1 + \frac{\alpha(r, z) - 1}{w(r, z)r} \frac{z^k - \hat{\mu}z^m}{\hat{t}} \right\}^{\frac{1}{\alpha(r, z) - 1}}. \quad (42)$$

By (41), the admissibility of ϕ^* requires

$$\int_{r=0}^{r=+\infty} \int_{z=0}^{z=+\infty} \left\{ \frac{\alpha(r, z) - 1}{w(r, z)} \right\}^{\frac{1}{\alpha(r, z) - 1}} r^{A - \frac{1}{\alpha(r, z) - 1} - 2} z^{\frac{\alpha(r, z)}{\alpha(r, z) - 1} k - q - 1} e^{-\frac{r}{B} - pz} dr < +\infty. \quad (43)$$

If we additionally assume that w is bounded and strictly positive, then (43) is reduced to

$$\int_{r=0}^{r=+\infty} \int_{z=0}^{z=+\infty} r^{A - \frac{1}{\alpha(r, z) - 1} - 2} z^{\frac{\alpha(r, z)}{\alpha(r, z) - 1} k - q - 1} e^{-\frac{r}{B} - pz} dr < +\infty, \quad (44)$$

and the condition (\mathbf{I}_k) is satisfied if

$$A - \frac{1}{\alpha(r, z) - 1} - 2, \frac{\alpha(r, z)}{\alpha(r, z) - 1} k - q - 1 \geq -1 + \delta \quad (45)$$

for a sufficiently small constant $\delta > 0$. Because (45) is rewritten as (the second inequality can be trivially satisfied by choosing a suitably smaller δ when necessary)

$$\alpha(r, z) \geq 1 + \frac{1}{A - \delta - 1} \quad \text{for } 0 < \delta < A - 1, \quad (46)$$

the generalized alpha divergence is suited to modeling uncertainties in the supOU process if α is sufficiently large. Because using a larger α results in a divergence that is less sensitive against uncertainties [30], one may use a state-dependent α by focusing on specific ranges of (r, z) . For example, in the context of modeling streamflow discharge, the focus may be high (large z) and/or prolonged (small r) flooding events. Similarly, one can also adaptively choose $w(r, z)$ under the same

idea for each given function α . If we assume that α is independent of z , then the argument analogous to that in **Proof of Proposition 2** predicts the tail behavior of the autocorrelation function as follows:

$$\text{ACF}(h) = O\left(h^{-\left(A - \frac{1}{\alpha_{r=0}-1}\right)}\right) \text{ for } h \gg 1, \quad (47)$$

showing that the ACF is predicted to be heavier in this case, and the heaviness becomes stronger for smaller α and hence for divergence closer to the KL one.

Second, we assume $0 < \alpha(\cdot, \cdot) < 1$. This is possibly an ill-posed case where the condition **(I_k)** is never satisfied. Indeed, the admissibility of ϕ^* requires

$$\int_{r=0}^{r=+\infty} \int_{z=0}^{z=+\infty} \max\left\{0, 1 - \frac{1 - \alpha(r, z)}{w(r, z)r} \frac{z^k - \hat{\mu}z^m}{\hat{\tau}}\right\}^{1 - \alpha(r, z)} r^{A-2} z^{k-q-1} e^{-\frac{r}{B} - pz} dr < +\infty \quad (48)$$

along with

$$1 - \frac{1 - \alpha(r, z)}{w(r, z)r} \frac{z^k - \hat{\mu}z^m}{\hat{\tau}} > 0 \text{ for all } r, z > 0. \quad (49)$$

The positivity condition (49) fails if the coefficient $\frac{1 - \alpha(r, z)}{w(r, z)}$ does not vanish for large z and small r . One may choose $w(r, z)$ so that this singularity is resolved while $\alpha(r, z)$ is strictly bounded between 0 and 1; however, this case needs a more complicated (and possibly difficult to interpret and extremely unsensitive) modeling strategy of w and α , and therefore our application in **Section 4** assumes $\alpha \geq 1$.

Finally, we move to the case $\alpha \equiv 1$, which corresponds to evaluating uncertainties by using a state-dependent KL divergence. By direct calculations, we have

$$\phi^*(r, z) = \exp\left\{\frac{1}{w(r, z)r} \frac{z^k - \hat{\mu}z^m}{\hat{\tau}}\right\}, \quad (50)$$

and the admissibility of ϕ^* requires

$$\int_{r=0}^{r=+\infty} \int_{z=0}^{z=+\infty} \exp\left\{\frac{1}{\hat{\tau}w(r, z)r} z^k\right\} r^{A-2} z^{k-q-1} e^{-\frac{r}{B} - pz} dr < +\infty. \quad (51)$$

This condition is insightful because it always fails if we assume a classical KL divergence (w is a constant function) irrespective of k due to the singular function $\frac{1}{r}$ in the exponential. This singularity issue for the classical KL divergence was reported earlier [30]. We can resolve this issue if $k=1$ by choosing w so that the function $\frac{1}{w(r, z)r}$ is bounded from above. The Musielak–Orlicz approach allows for such a

flexible modeling strategy, e.g., one may set

$$\frac{1}{w(r, z)r} = \frac{1 - e^{-Wr}}{cr} \text{ or equivalently } w(r, z) = \frac{c}{1 - e^{-Wr}} \quad (52)$$

with constants $c, W > 0$. This w gives a strictly bounded $1/(wr) \leq W$ and resolves the singularity issue caused by $1/r$ using the regularization near $r = 0$. The strength of this regularization can be controlled by $W > 0$ in such a way that a larger W means a weaker regularization effect, and there is no regularization under the limit $W \rightarrow +\infty$. One can also consider a z -dependent w if it remains bounded and does not encounter the singularity issue at $r = 0$, implying versatility of the present approach based on Musielak–Orlicz spaces. In this case, because there is no singularity of ϕ^* at $r = 0$, the tail behavior in **Proposition 2** does not change, which is the case for our computation in **Section 4**. We computationally found that $\hat{\tau}$ is sufficiently large such that the condition (51) is satisfied.

We briefly discuss the **Lower bound case** where the classical KL divergence does not fail because of

$$\phi^*(r, z) = \exp \left\{ \frac{-1}{w(r, z)r} \frac{z^k - \hat{\mu}z^m}{\hat{\tau}} \right\}, \quad (53)$$

which satisfies the condition **(Ik)**, and hence, we can choose w as a constant in this case. The tail of the autocorrelation function of the distorted model does not change with w given by (52). If $\alpha(\cdot, \cdot) > 1$, we have

$$\phi^*(r, z) = \max \left\{ 0, -\frac{\alpha(r, z) - 1}{w(r, z)r} \frac{z^k - \hat{\mu}z^m}{\hat{\tau}} + 1 \right\}^{\frac{1}{\alpha(r, z) - 1}}, \quad (54)$$

and the condition **(Ik)** is always satisfied if $z^{k-m} \in L_{\hat{\Psi}}$ due to $\hat{\mu} \leq 0$.

3.3 Computational method

By **Propositions 4-5**, we can solve the optimization problems by using a gradient descent method for the Lagrangian multipliers μ, τ . We are aiming to present a simple computational method for our optimization problems but not to compare algorithms.

For the **Upper-bound case**, we want to find a solution $(\hat{\tau}, \hat{\mu})$, optimal Lagrangian multipliers, to the following coupled system (34), where by elementary calculations,

$$\frac{\partial F(\tau, \mu)}{\partial \tau} = \frac{\varepsilon}{mc_m} - \mathbb{E}_m \left[\Phi \left(w', \alpha, \frac{\partial \Psi}{\partial \psi} \left(w', \alpha, \frac{z^{k-m} - \mu}{\tau} \right) \right) \right], \quad (55)$$

$$\frac{\partial F(\tau, \mu)}{\partial \mu} = \tau \left\{ 1 - \mathbb{E}_m \left[\frac{\partial \Psi}{\partial \psi} \left(w'(r, z), \alpha(r, z), \frac{z^{k-m} - \mu}{\tau} \right) \right] \right\}. \quad (56)$$

Here, the partial derivative $\frac{\partial \Psi}{\partial \psi}$ is taken with respect to the third argument. A difficulty in solving the

system (34) is that the partial derivatives $\frac{\partial F}{\partial \tau}$ and $\frac{\partial F}{\partial \mu}$ are not globally Lipschitz continuous, which is often assumed to safely implement gradient descent methods and their variants [55-57]. The loss of the

Lipschitz continuity of partial derivatives is due to the appearance of the term $\frac{z^{k-m} - \mu}{\tau}$. Nevertheless,

because the system (34) admits an interior solution (**Proposition 3**), we have $(\hat{z}, \hat{\mu}) \in [L^{-1}, L] \times [L^{-1}, L]$ with some sufficiently large constant $L > 0$, and the partial derivatives of F are Lipschitz continuous in this domain. We implement a gradient method with momentum to solve (34), as shown in **Section A2 in Appendix** with a convergence study.

We need to discretize expectations appearing in each partial differential in (34) to fully implement the gradient descent method. We apply the quantization method (Proof of Proposition 2 in Yoshioka [58]). Note that the probability measure p_m is decomposable to the two probability measures $\pi_m = c_1 r^{-1} \pi$ and $\nu_m = c_2 z^m \nu$ with normalization constants c_1, c_2 . Fix the computational resolution $M \in \mathbb{N}$, and set the quantiles $P_{i,M}$ and $Q_{i,M}$ that uniformly discretize π_m, ν_m as follows:

$$\frac{i}{M} = \int_0^{P_{i,M}} \pi_m(dr) \quad \text{and} \quad \frac{i}{M} = \int_0^{Q_{i,M}} \nu_m(dv), \quad i = 0, 1, 2, \dots, M. \quad (57)$$

Then, we set $x_{i,M} = P_{2i-1,2M}$ and $y_{i,M} = Q_{2i-1,2M}$ ($i = 1, 2, 3, \dots, M$). This quintile approximation has the pointwise error M^{-1} between the discretized and true cumulative distributions of a probability measure that admits a density (Proof of Proposition 2 in Yoshioka [58]). We apply the following rule to discretize each expectation appearing in (55)-(56): for generic $f : (0, +\infty)^2 \times \mathbb{R} \rightarrow \mathbb{R}$,

$$\mathbb{E}_m \left[f \left(w'(r, z), \alpha(r, z), \frac{z^{k-m} - \mu}{\tau} \right) \right] \approx \frac{1}{M} \sum_{i,j=1}^M f \left(w'(x_{i,M}, y_{j,M}), \alpha(x_{i,M}, y_{j,M}), \frac{(y_{j,M})^{k-m} - \mu}{\tau} \right). \quad (58)$$

Finally, we can numerically solve the **Lower-bound case** in the same way by the formal replacement $F \Rightarrow G$ in the explanation above, where

$$\frac{\partial G(\tau, \mu)}{\partial \tau} = \frac{\varepsilon}{mc_m} - \mathbb{E}_m \left[\Phi \left(w', \alpha, \frac{\partial \Psi}{\partial \psi} \left(w', \alpha, \frac{-z^{k-m} - \mu}{\tau} \right) \right) \right], \quad (59)$$

$$\frac{\partial G(\tau, \mu)}{\partial \mu} = \tau \left\{ 1 - \mathbb{E}_m \left[\frac{\partial \Psi}{\partial \psi} \left(w'(r, z), \alpha(r, z), \frac{-z^{k-m} - \mu}{\tau} \right) \right] \right\}. \quad (60)$$

Remark 7 When $m = 0$, it suffices to formally fix $\mu = 0$ and simply find a minimizing τ , where the functions F and G are convex. The mathematical and computational approaches for $m \geq 1$ carry over to this case with proper simplifications.

4. Application

4.1 Data description

The supOU process (1) along with the optimization problems (13)-(14) are applied to real data. We use the hourly streamflow discharge data of a Class-A River in a mountainous Hakusan area, Hakusan City,

Ishikawa Prefecture, Japan (Kazarashi station: 36.16778 N, 136.63194 E, with an elevation of 494.0 (m)). Temporally fine (e.g., hourly to daily) streamflow discharge and its fluctuation have been suggested to exhibit long memory [e.g., 15,48,59-63]. River waters in this area have been serving as a water resource for residents [64] and local industries such as Tofu production and aquaculture of inland fish species. A dominant source of the long memory of the river water in the study area is considered to be shallow groundwater supply and the melting of snowpack accumulation, but their detailed estimations have not been conducted thus far. Moreover, the study area has been suggested to experience an increased probability of annual flood occurrence under future climate change [65,66] and the increase in the temporal variability of streamflow discharge under the regional warming scenarios [67], motivating us to investigate supOU processes subject to model uncertainties.

The hourly discharge data have been measured at Kazarashi station by the Ministry of Land, Infrastructure, Transport and Tourism; but recently, most parts of the data are “missing”, at least from June to July in 2023, probably due to technical reasons such as the failure of observation equipment², and future changes in streamflow characteristics under climate change are considered important. We collected hourly discharge data from April 1, 2016 to March 31, 2023 at Kazarashi station² considering data availability (most parts of the data are “missing” in January to March in 2016, and in total 61,344 data points exist and 577 of them are missing). **Figure 1** shows the streamflow discharge data used in this paper. **Figure 2** compares the empirical and theoretical autocorrelation functions of the discharge data. We identified a classical supOU process with reversion and Lévy measures by assuming (39) and (40) by using a moment-matching method that has already been validated in previous studies [e.g., 68], along with a comparison between empirical and theoretical cumulants (**Table 1**). As shown in **Table 1**, the streamflow discharge at this station has a long-memory property because the parameter A , the Hurst index, is approximately 1.5, and this characteristic is captured by the theory (**Figure 2**).

² Water Information system. <http://www1.river.go.jp/cgi-bin/SiteInfo.exe?ID=304111284412020> (In Japanese. Last Accessed on February 24, 2026)

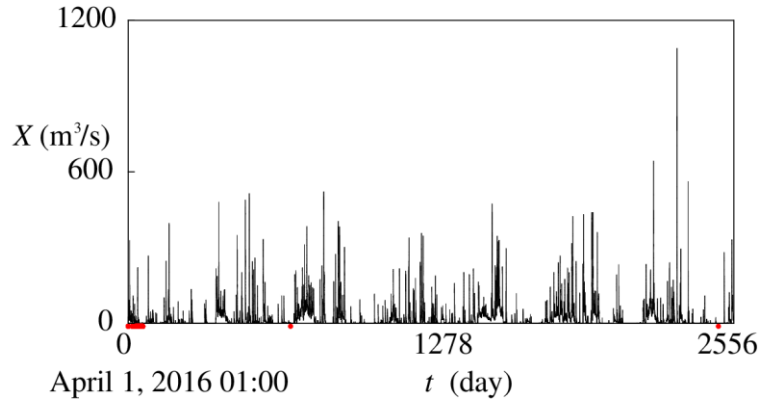


Figure 1. Discharge data at Kazarashi station. Red circles represent the time points with missing data.

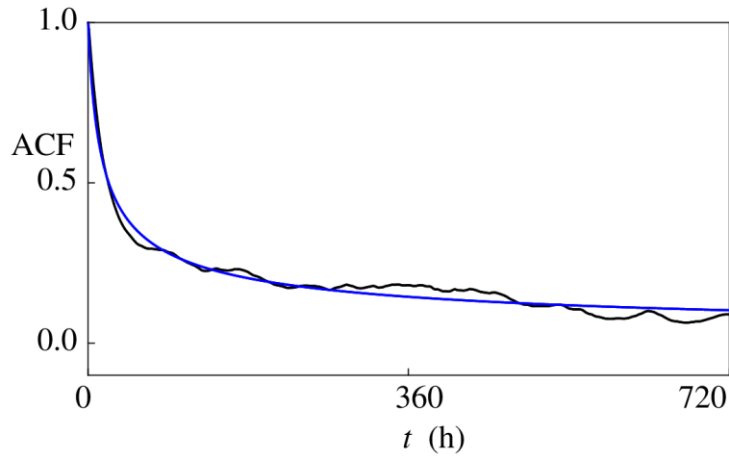


Figure 2. Autocorrelation function (ACF) at Kazarashi station. The black curve represents the empirical ACF, and the blue curve represents the theoretical ACF.

Table 1. Theoretical parameter values cumulants. The values inside “(,)” represent empirical cumulants and their relative errors.

A (-)	1.502.E+00
B (1/h)	1.282.E-01
c_v ($m^{3q} / s^q / h$)	2.856.E-03
p (s/m^3)	7.474.E-03
q (-)	-2.429.E-01
Average (m^3/s)	1.771.E+01 (1.757.E+01, 7.899.E-03)
Variance (m^6/s^2)	1.472.E+03 (1.478.E+03, 3.996.E-03)
Skewness (-)	5.214.E+00 (4.977.E+00, 4.750.E-02)
Kurtosis (-)	4.421.E+01 (4.518.E+01, 2.135.E-02)

4.2 Computational setting

We compute the optimization problems in the **Upper- and Lower-bound cases** for different Φ . We first use the following alpha divergence function:

$$\Phi(w(r), \alpha(r), x) = w(r) \frac{x^{\alpha(r)} - \alpha(r)(x-1) - 1}{\alpha(r)(\alpha(r)-1)}, \quad r, z > 0 \text{ and } x > 0, \quad (61)$$

where $\alpha(\cdot) > 1$ is a constant or continuous function of r to account for the importance of reversion rates, namely, timescales. For the visualization of Φ and its convex conjugate Ψ , see **Figures 3-4**. The weight w is given by (52) so that the singularity at $r=0$ is regularized due to facing some computational instability in the gradient descent method, which is considered because of the appearance of very large expectants in (55)-(56). The constant $c > 0$ is determined to normalize the weight as $\int_0^{+\infty} \int_0^{+\infty} w'(r, z) \pi(dr) \nu(dz) = 1$. The weight w in (52) is valid if the memory structure of X is not critically affected by uncertainties, which is assumed in **Section 4** for modeling simplicity. Recall that, even in this simplified setting, $w'(r, z)$ depends both on r and z . We investigate the behavior of Lagrangian multipliers and solutions to the optimization problems under (61). For this case, we set $(m, k) = (1, 2)$ and examine $\varepsilon = 10^{2-0.6i}$ ($i = 0, 1, 2, \dots, 10$), and the error threshold for convergence is $\delta = 10^{-5}$.

We also consider the following weighted KL divergence:

$$\Phi(w(r), x) = w(r)(x \ln x - x + 1), \quad r, z > 0 \text{ and } x > 0, \quad (62)$$

where w is given by (52) and $c > 0$ is the constant for the normalization. This case is interesting by itself, and moreover, it gives the following interpretation of the reversion and Lévy measures:

$$\phi^*(r, z) \pi(dr) \nu(dz) = \underbrace{\pi(dr)}_{\substack{\text{Reversion measure} \\ \text{(Not modified)}}} \times \underbrace{\exp\left(\pm \frac{c(1-e^{-Wr})}{\hat{r}} z\right)}_{\substack{\text{r-dependent tempered-stable Lévy measure}}} \nu(dz), \quad r, z > 0, \quad (63)$$

where the distorted Lévy measure is again of the tempered-stable type that is now inhomogeneous (40), which is computationally advantageous in our case; **Table 1** suggests that the Lévy measure ν in the present case is of the compound Poisson type with jumps distributed according to a gamma distribution. Therefore, with the formula (63), jumps can be generated by gamma distributions depending on r . We compute the supOU process (1) by using a discrete superposition scheme, which itself is not new but simple to implement. We discretize (1) for $r > 0$ as follows based on the representation formula of supOU processes (e.g., Proposition 1 in Fasen and Klüppelberg [51]; Eqs. (63)-(64) in Yoshioka [58]):

$$X_t \approx \sum_{i=1}^M X_t^{(i)} \quad \text{with} \quad dX_t^{(i)} = -r_i X_t^{(i)} dt + dZ_t^{(i)}, \quad (64)$$

where each of $Z^{(i)}$ are mutually-independent jump processes with the Lévy measures $\frac{1}{B(A-1)} r_i M^{-1} \phi^*(r_i, z) \nu(dr)$ with each r_i being generated by the quantization (57) with the formal

replacement $A \rightarrow A-1$ in (39) and suitably updating the normalization constant c_π , and each $X^{(i)}$ is computed using a common Euler–Maruyama time discretization and jumps are generated by an acceptance-rejection method. For the present case, we set $(m, k) = (0, 1)$ and examine $\varepsilon = 10^{1-0.6i}$ ($i = 0, 1, 2, \dots, 10$), and the error threshold for convergence is $\delta = 10^{-7}$. We compute threshold crossing dynamics of the supOU process at different ε as explained later. The time increment for sampling each supOU process is 1/100 (h), and we simulate each sample path for 2,000 (yr) with a burn-in period of 2000 (yr) with a time increment of 1 (h).

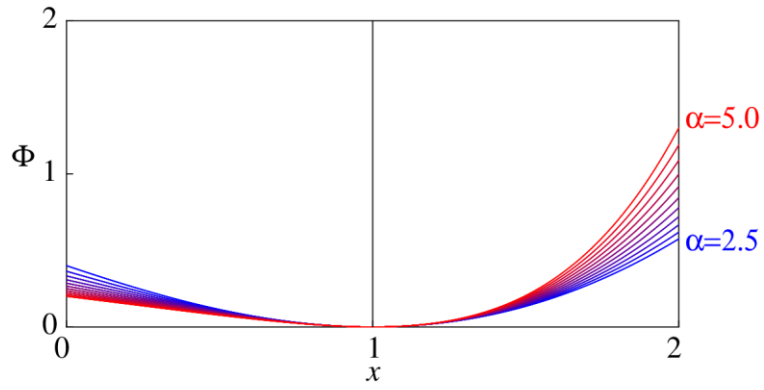


Figure 3. Homogeneous (w' is replaced by 1 and α by a constant) divergence function $\Phi = \Phi(x)$ for $\alpha = 2.5i$ ($i = 0, 1, 2, \dots, 10$).

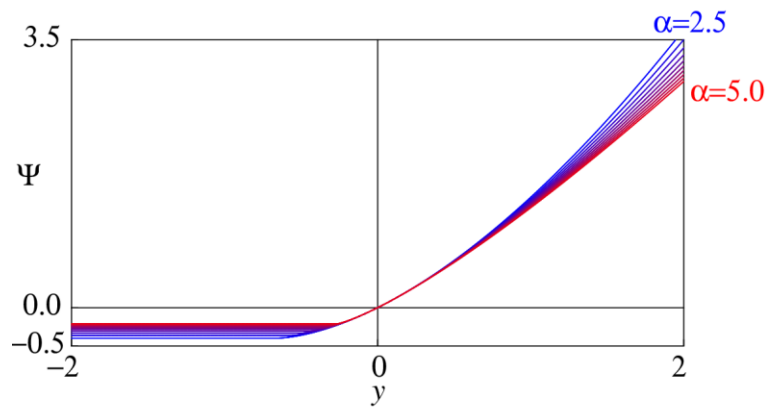


Figure 4. Convex divergence $\Psi = \Psi(y)$ of the homogeneous Φ in **Figure 3** for $\alpha = 2.5i$ ($i = 0, 1, 2, \dots, 10$).

4.3 Results and discussion

4.3.1 Parameter dependence on the optimization problems

We examine three constant α cases $\alpha \equiv 2.5, 4.0, 5.0$ and two state-dependent α cases

$$\alpha(r) = 2.5 + (5.0 - 2.5) \min\{1, r\} \quad \text{and} \quad \alpha(r) = 5.0 + (2.5 - 5.0) \min\{1, r\}, \quad (65)$$

which are called the increasing and decreasing cases, respectively. We choose the regularization parameter value of $W = 10$ (h), and the influences of W are discussed in **Section A3** in **Appendix**.

Figures 5-7 show the computed variances, $\hat{\tau}$, and $\hat{\mu}$ for each case. **Figure 5** for the variance under distortion shows that, in the **Upper-bound case**, specifying smaller α values yields a more pessimistic overestimation of the variance at each ε . For the inhomogeneous α , their results are between those of $\alpha \equiv 2.5, 5.0$, possibly due to the formulation (65), but the increasing and decreasing cases give distinctive results. The increasing case (resp., decreasing case) is more pessimistic for smaller (resp., larger) reversion rates r and gives results closer to that of $\alpha \equiv 2.5$ (resp., $\alpha \equiv 5.0$). A smaller r corresponds to slowly decaying streamflow discharge, such as groundwater recharge to the river (e.g., baseflow), and this is where the weight w' becomes large. Evaluation of the state-dependence, which is based on Musielak–Orlicz spaces, allows for this inhomogeneity in r . The computational results for the **Lower bound case** are not significantly different among the cases examined here, suggesting higher sensitivity in the **Upper bound case** against α and hence the corresponding Musielak–Orlicz spaces.

Figure 6 for the optimal Lagrangian multiplier $\hat{\tau}$ about the constraint of divergence shows that they are decreasing in ε for all computational cases. This implies that perturbing the divergence constraint affects the objective more for larger ε values, implying that tightening the uncertainty set rapidly decreases the objective for larger uncertainty sets (Chapter 5.6.2 in Boyd and Vandenberghe [44]). **Figure 7** for the optimal Lagrangian multiplier $\hat{\mu}$ about the constraint of average shows that $\hat{\mu}$ is not monotone with respect to ε ; for the **Upper-bound case**, the monotonicity appears at approximately ε values of 1 to 10, corresponding to the variance values doubling the benchmark value. For the **Lower-bound case**, the monotonicity appears at approximately ε values of 0.001 to 0.1, with the variance values closer to (difference is smaller than a few percent of) the benchmark value. The reasons for these non-monotone profiles are not theoretically clear but are considered due to the problem setting except for the divergences because they commonly appear in the computational cases examined here. For $\hat{\mu}$, **Figure 6** suggests that perturbing the constraint about the average discharge constraint has larger impacts on the objective for smaller ε values, which is in contrast to the role of $\hat{\tau}$.

The conditional cumulative distributions of p_m for r and z values are denoted as F_r and F_z , which range from 0 to 1 as r and z increase from 0 to $+\infty$, respectively. **Figures 8-9** show the computed optimizers ϕ^* for the increasing case for the **Upper- and Lower-bound cases**, respectively. Decreasing ε results in ϕ^* closer to the constant function $\phi^* \equiv 1$ because smaller distortion is allowed. For the **Upper-bound case**, as shown in **Figure 8**, ϕ^* attains large values for large $F_z > 0.8$, which

corresponds to the tail probability of jumps, implying that model uncertainties are judged due to the distortion of tails in the proposed mathematical framework. This implies that the pessimistic increase in streamflow discharge is due to the increase in the magnitude and frequency of large flood events rather than small flood events. Moreover, higher ϕ^* for large z and small r values imply that the overestimation of baseflow events also contributes to the increase in streamflow variability; this point is consistent with the discussion for **Figure 5** of the variance under uncertainties. In contrast, for the **lower-bound case**, as shown in **Figure 9**, ϕ^* attains large values for small Fz , suggesting that the pessimistic decrease in streamflow discharge is due to the decrease in base flows and flood events. In **Figures 8-9**, the heterogeneity of ϕ^* for the reversion speed r seems rather weak compared to that of jumps z . For both **Upper- and lower-bound cases**, the optimal ϕ^* has more localized profiles for larger ε values. The analysis of ϕ^* thus provides how the worst-case model uncertainties distort the reversion and Lévy measures.

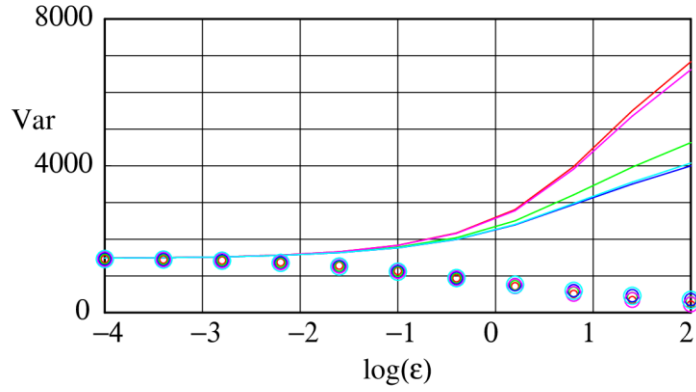


Figure 5. Computed variance (Var) (m^6/s^2) values of the distorted supOU processes for different values of ε in **Upper-bound case** (curves) and **Lower-bound case** (circles). Colors represent $\alpha \equiv 2.5$ (red), $\alpha \equiv 4.0$ (green), $\alpha \equiv 5.0$ (blue), increasing α (magenta), and decreasing α (sky blue).

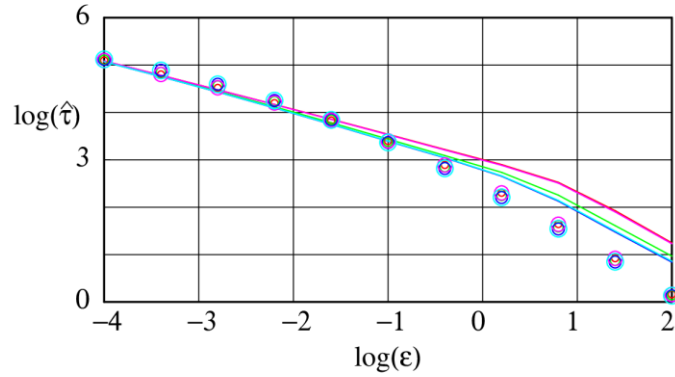


Figure 6. Computed $\tau = \hat{\tau}$ (m^6/s^2) values of the distorted supOU processes for different values of ε in **Upper-bound** and **Lower-bound cases**. Same color legend as in **Figure 5**.

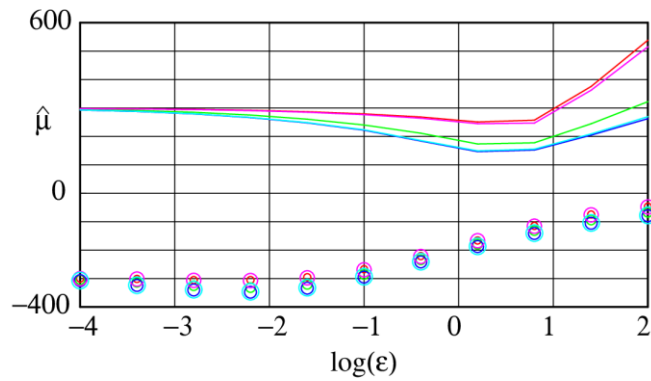


Figure 7. Computed $\mu = \hat{\mu}$ (m^3/s) values of the distorted supOU processes for different values of ε in **Upper-bound** and **Lower-bound cases**. Same color legends as in **Figure 5**.

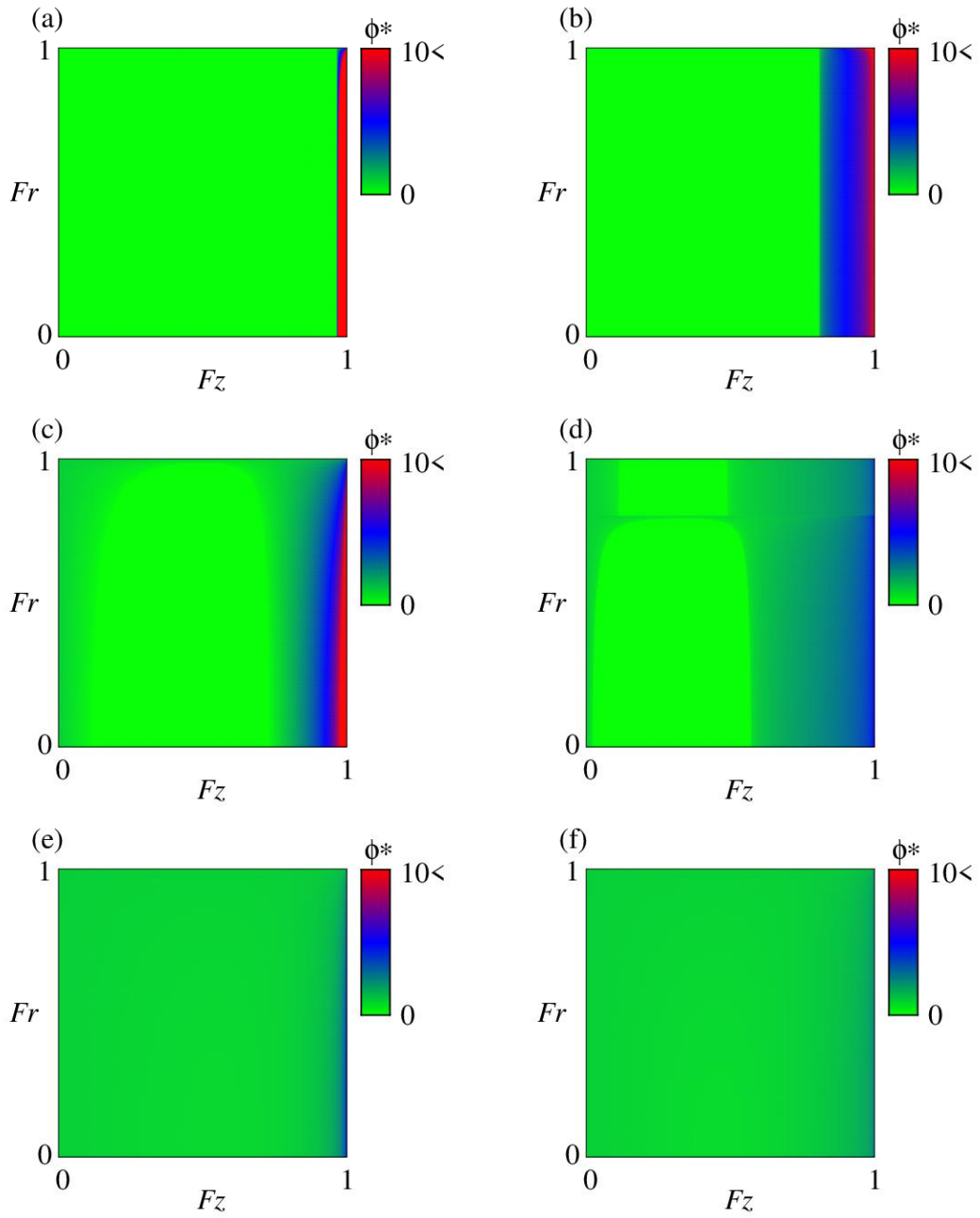


Figure 8. Computed ϕ^* in **Upper-bound case** with increasing and decreasing α : (a) increasing with $\varepsilon = 100$, (b) decreasing with $\varepsilon = 100$, (c) increasing with $\varepsilon = 6.31$, (d) decreasing with $\varepsilon = 6.31$, (e) increasing with $\varepsilon = 0.1$, (f) decreasing with $\varepsilon = 0.1$.

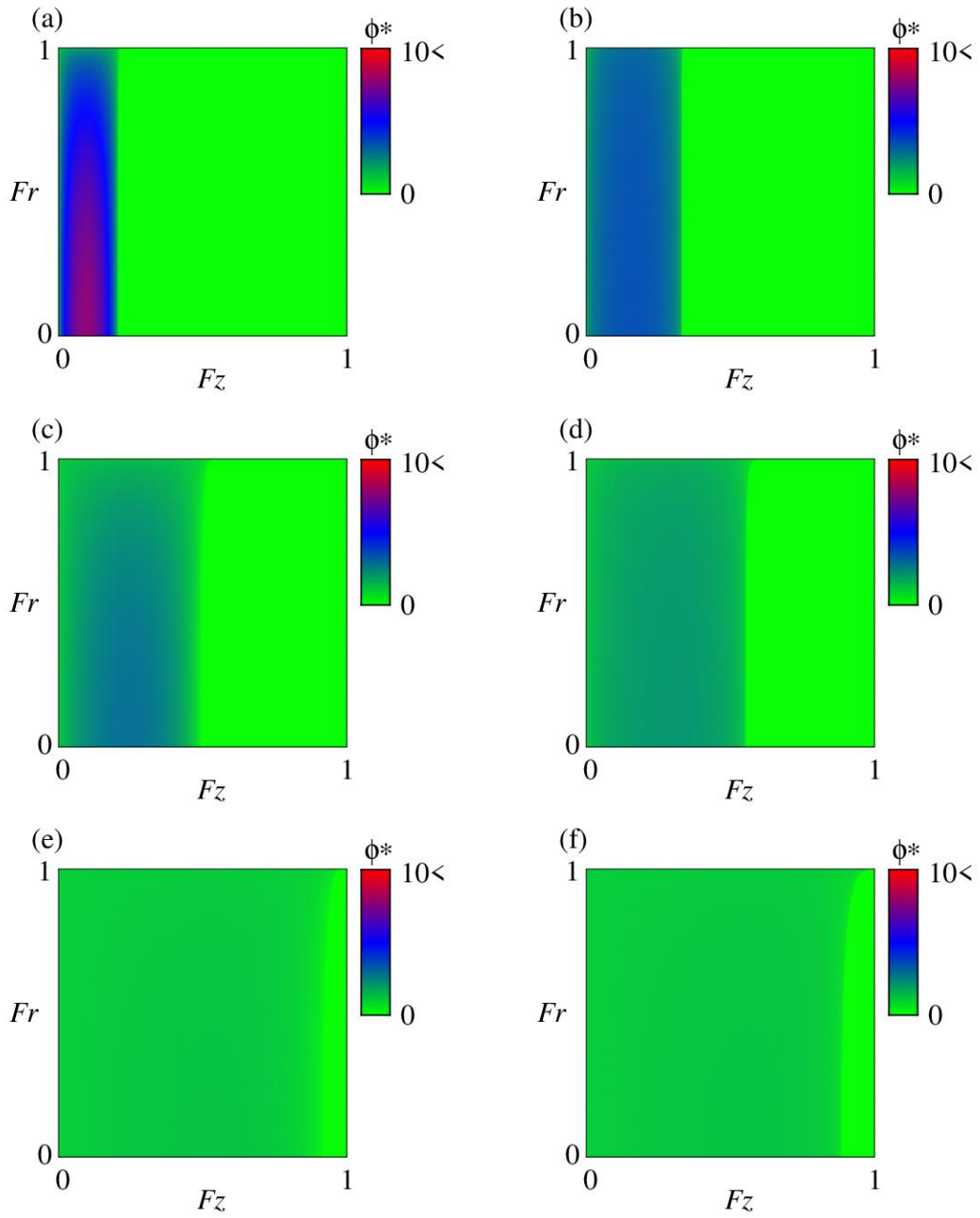


Figure 9. Computed ϕ^* in **Lower bound case** with increasing and decreasing α : (a) increasing with $\varepsilon = 100$, (b) decreasing with $\varepsilon = 100$, (c) increasing with $\varepsilon = 6.31$, (d) decreasing with $\varepsilon = 6.31$, (e) increasing with $\varepsilon = 0.1$, (f) decreasing with $\varepsilon = 0.1$.

4.3.2 Distorted supOU processes

We computationally simulate the supOU processes for **Upper- and Lower-bound cases** by focusing on threshold crossing dynamics. Streamflow discharge itself as a continuous-state variable is of importance in hydrology, while its threshold statistics, such as high- and low-flow periods, also play roles in engineering applications such as sand and gravel transport as well as their efficient [69,70] and plant uprooting [71,72], both of which are suggested to occur only during high-flow durations. Statistical analysis of flow durations would also be important for freshwater fish species such as salmonids, some of which are found in the mountains reaches in the Tedor River [73]. Moreover, too little streamflow discharge would be critical for water-intake facilities such as those for hydropower generation [74], which is also the case around Kazarashi station³.

Here, a high-flow period (resp., low-flow period) means a period during which the streamflow discharge is larger than (resp., not larger than) a prescribed threshold value $X_{\text{thr}} > 0$. Statistics of these periods can be computed by sampling from a sufficiently long sample path of streamflow discharge generated from a model and are inevitably affected by model uncertainties. We study the influences of model uncertainties on the statistics of high- and low-flow periods.

The averages of streamflow discharge for selected cases are presented in **Table 2**, which are used in the sequel for sensitivity analysis. These cases correspond to $\varepsilon = O(10^{-1})$, where the average values of the distorted models are approximately $\pm 50\text{-}60\%$ and $\pm 20\text{-}30\%$ of the benchmark values, which are considered within a reasonable range considering the variations in annual average values at the study site. **Figure 10** shows computed one-year sample paths for the benchmark case and **Upper- and Lower-bound cases** with $\varepsilon = 0.631$, suggesting that the overestimation of average discharge increases both minimum and maximum discharges, and vice versa. **Figure 11** shows the computed averages of the distorted supOU processes for different values of ε in **Upper- and Lower-bound cases**. We focus later on the two cases $X_{\text{thr}} = 20$ (m³/s) (quantile level 77.9% with the benchmark model) and $X_{\text{thr}} = 160$ (m³/s) (quantile level 98.4% with the benchmark model); the former corresponds to the value closely linked to the threshold for hydropower intake where the water cannot be intake during low-flow periods, while the latter corresponds to flood events where there may be flood disturbances on the aquatic environment and ecosystems of the river.

Figure 12 compares the computed PDFs of the streamflow discharge among the empirical and distorted supOU processes. **Figures 13-14** show the PDFs of the durations of the high- and low-flow periods, respectively. **Table 3** summarizes the average and variance for high-flow periods with $X_{\text{thr}} = 20$ (m³/s) computed by the benchmark and distorted model as a representative case. Similarly, **Table 4** summarizes the results for low-flow periods. **Tables 5-6** show the results with $X_{\text{thr}} = 160$ (m³/s) as a representative case of a larger threshold value. The tails of the PDFs of streamflow discharge become heavier as the

³Tedori River Project Overview <https://www.hrr.mlit.go.jp/kanazawa/chisui/doc/tedori.pdf> (In Japanese. Last accessed on March 4, 2026)

average discharge is more strongly overestimated, as shown in **Figure 12(b)**. In contrast, as shown in **Figure 12(a)**, the maximum of the PDF near the origin becomes larger as the average discharge is more strongly underestimated. In these views, the computational results demonstrate how the discharge PDF is distorted under the worst-case uncertainties. **Figures 13-14** suggest that the statistical properties of the durations of high- and low-flow periods do not change qualitatively by assuming model uncertainties in our framework but are different quantitatively.

Because a supOU process is a non-Markovian model that is not necessarily efficiently computable due to superposing OU processes, the computational cost at least linearly scales with the degree of freedom in the r direction. Model reduction focusing on a threshold discharge potentially allows modeling high- and low-flow periods in a simpler way, which can be approximated Markovian if they are considered generated by exponential distributions. Recall that the exponential distribution has the PDF $\lambda e^{-\lambda w}$ ($w > 0$), where both the mean and standard deviation are λ^{-1} , and hence, the coefficient of variation is 1. In this view, **Tables 3 and 6** suggest that durations of low-flow periods can be reasonably fitted with exponential distributions with λ^{-1} (h) being identified as the average duration for all the computational cases, serving as a reasonable model reduction with capturing the empirical tails (**Figure 14**); however, the same seems not to be true for high-flow periods where the coefficient of variation is approximately 3 to 6, which are significantly larger than 1. This implies that the non-Markovian nature of both benchmark and distorted supOU processes appear in modeling the high-flow periods, particularly the fat tails of the PDFs of their durations, which would not be captured by exponential distributions.

A minimum model for durations of the high-flow periods with fat tails would be the following inverse-gamma distribution:

$$c'(Y)^{-\zeta-1} \exp\left(-\frac{1}{\mathcal{G}\zeta}\right), Y > 0 \quad (66)$$

with the normalization constant $c' > 0$, shape parameter ζ (-) and scaling parameter \mathcal{G} (day). This PDF has a tail that behaves asymptotically as $Y^{-\zeta-1}$ for large $Y > 0$. Theoretical and empirical averages and variances are equalized to estimate the parameters $\zeta (> 2)$ and \mathcal{G} (e.g., Table 2 in Yoshioka et al. [75]).

Applying a moment-fitting by using the computed average and variance of high-flow periods uniquely gives the estimated values of the parameters ζ and \mathcal{G} , with the former being closed to 2 (**Tables 7-8**). **Table 9** then shows the percentages of the occurrence of high-flow periods for different values of X_{thr} , which suggests how the durations of high-flow periods (and hence low-flow periods) are affected by model uncertainties. The fitted PDFs of the durations of each period are shown in **Figure 13**, suggesting a reasonable agreement between the empirical and fitted results with a slight underestimation of the empirical tails. These PDFs, which have fat tails, correspond to the long-memory nature of the underlying (distorted) supOU processes. This implies that the two-state reduced modeling of the streamflow discharge of a supOU process with long memory needs a couple of exponential and nonexponential distributions. Indeed, if a

random variable Y follows the inverse-gamma distribution (66), then its inverse $Y' = Y^{-1}$, which in our context represents the reversion rate of high-flow periods, follows the gamma distribution of the shape parameter ζ and scaling parameter ϑ . This PDF has a singularity at the origin of the form $(Y')^{\zeta-1}$.

Tables 7-8 show that the fitted values of ζ are at most $2 + O(10^{-2})$, demonstrating that durations of high-flow periods involve a wide range of timescales corresponding to the long memory nature of the supOU processes. The parameter ζ therefore represents the degree of non-Markovian nature, and its values are almost the same across the different computational cases with different ε values. This is consistent with our theoretical finding that the weight w is regularized with which the memories of the distorted supOU processes are qualitatively the same. As demonstrated above, the methodology proposed in this paper can be used to analyze various aspects of the supOU processes.

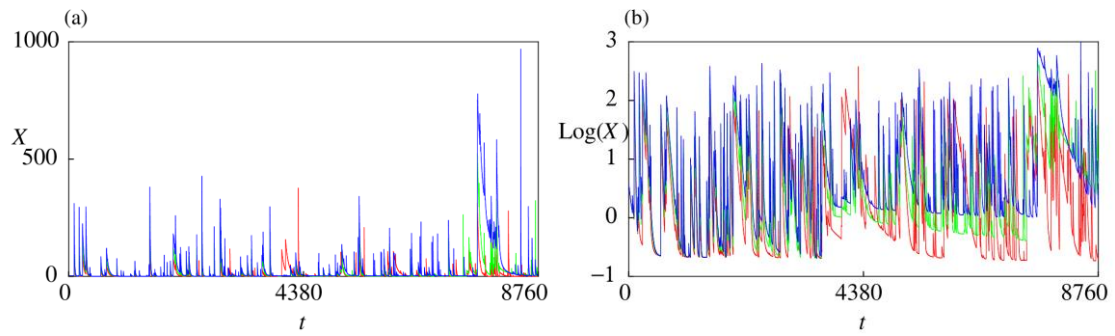


Figure 10. One-year ($0 \leq t \leq 8760$ (h)) sample paths of the discharge X (m^3/s) on the (a) ordinary and (b) common logarithmic scales: the benchmark case (green), **Upper-bound case** with $\varepsilon = 0.631$ (blue), and **Lower-bound case** with $\varepsilon = 0.631$ (red).

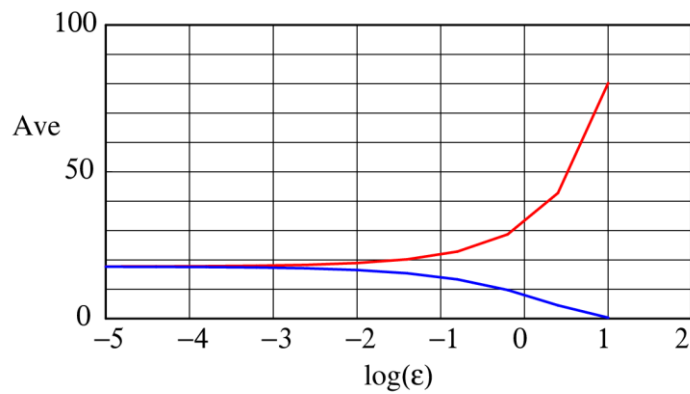


Figure 11. Computed average (Ave) (m^3/s) values of the distorted supOU processes in **Upper-bound case** (red) and **Lower-bound case** (blue).

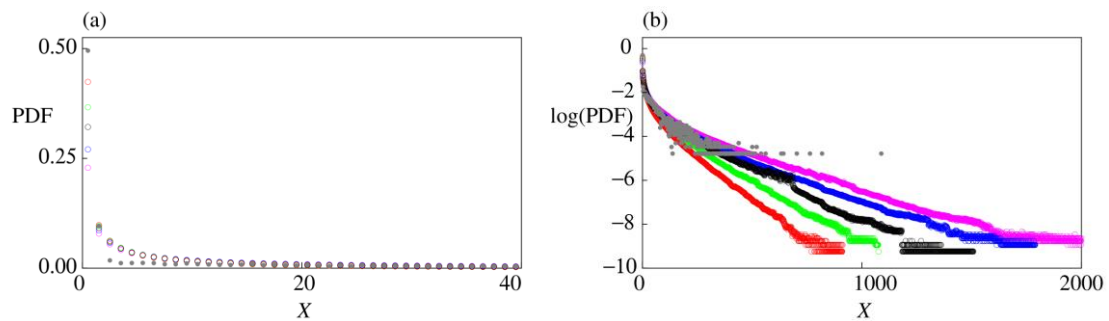


Figure 12. Comparison of the PDFs of streamflow discharge X (m^3/s) among the empirical data and computational results on (a) ordinary scale and (b) common logarithmic scale: empirical data (gray), benchmark case (black), **Lower-bound case** with $\varepsilon = 0.631$ (red), **Lower-bound case** with $\varepsilon = 0.159$ (green), **Upper-bound case** with $\varepsilon = 0.159$ (blue), and **Upper-bound case** with $\varepsilon = 0.631$ (magenta).

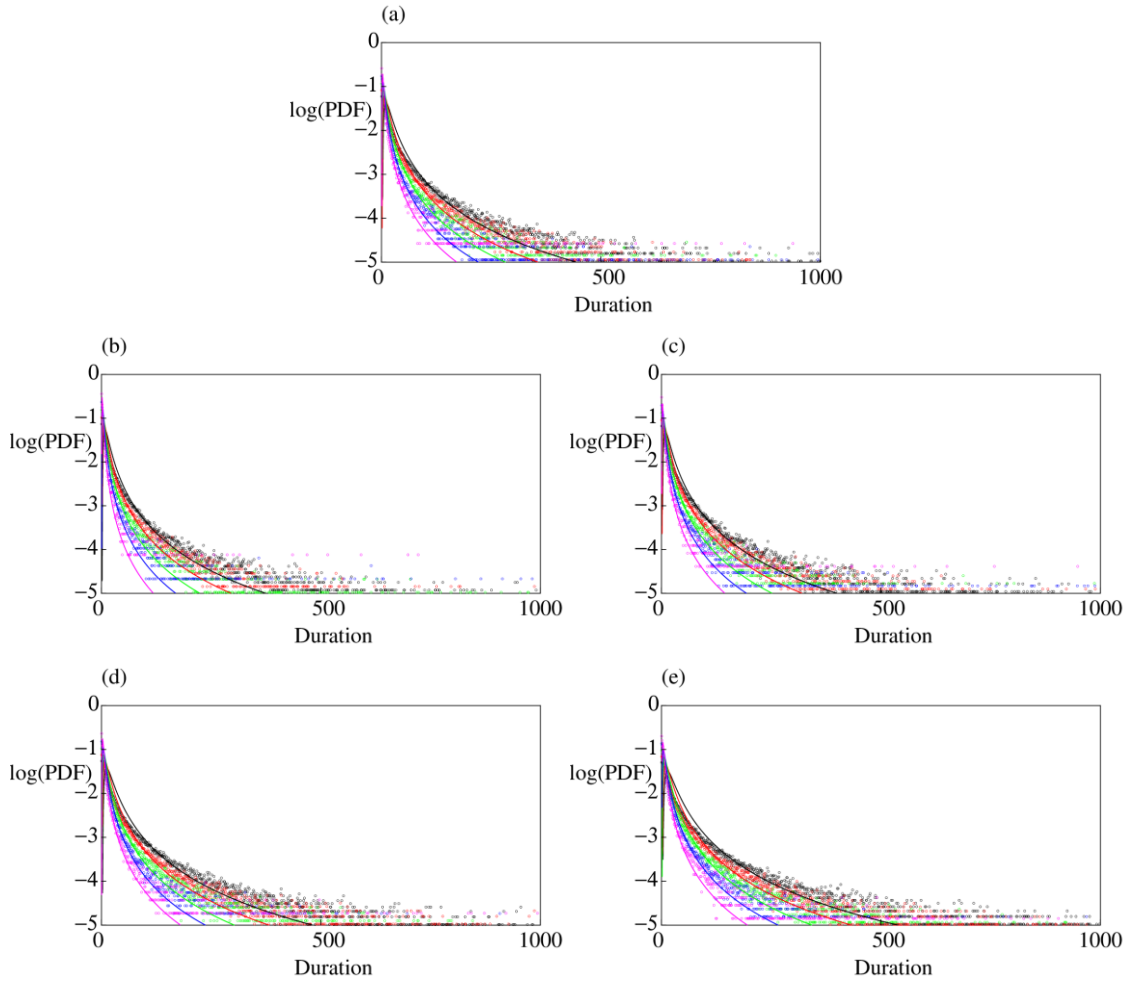


Figure 13. Comparison of the PDFs in the common logarithmic scale for durations (h) of the high-flow periods, where circles and curves represent empirical and fitted results, respectively: (a) Benchmark case, (b) **Lower-bound case** with $\varepsilon = 0.631$, (c) **Lower-bound case** with $\varepsilon = 0.159$, (d) **Upper-bound case** with $\varepsilon = 0.159$, (e) **Upper-bound case** with $\varepsilon = 0.631$. Color legends represent $X_{\text{thr}} = 10$ (m³/s) (black), $X_{\text{thr}} = 20$ (m³/s) (red), $X_{\text{thr}} = 40$ (m³/s) (green), $X_{\text{thr}} = 80$ (m³/s) (blue), and $X_{\text{thr}} = 160$ (m³/s) (magenta).

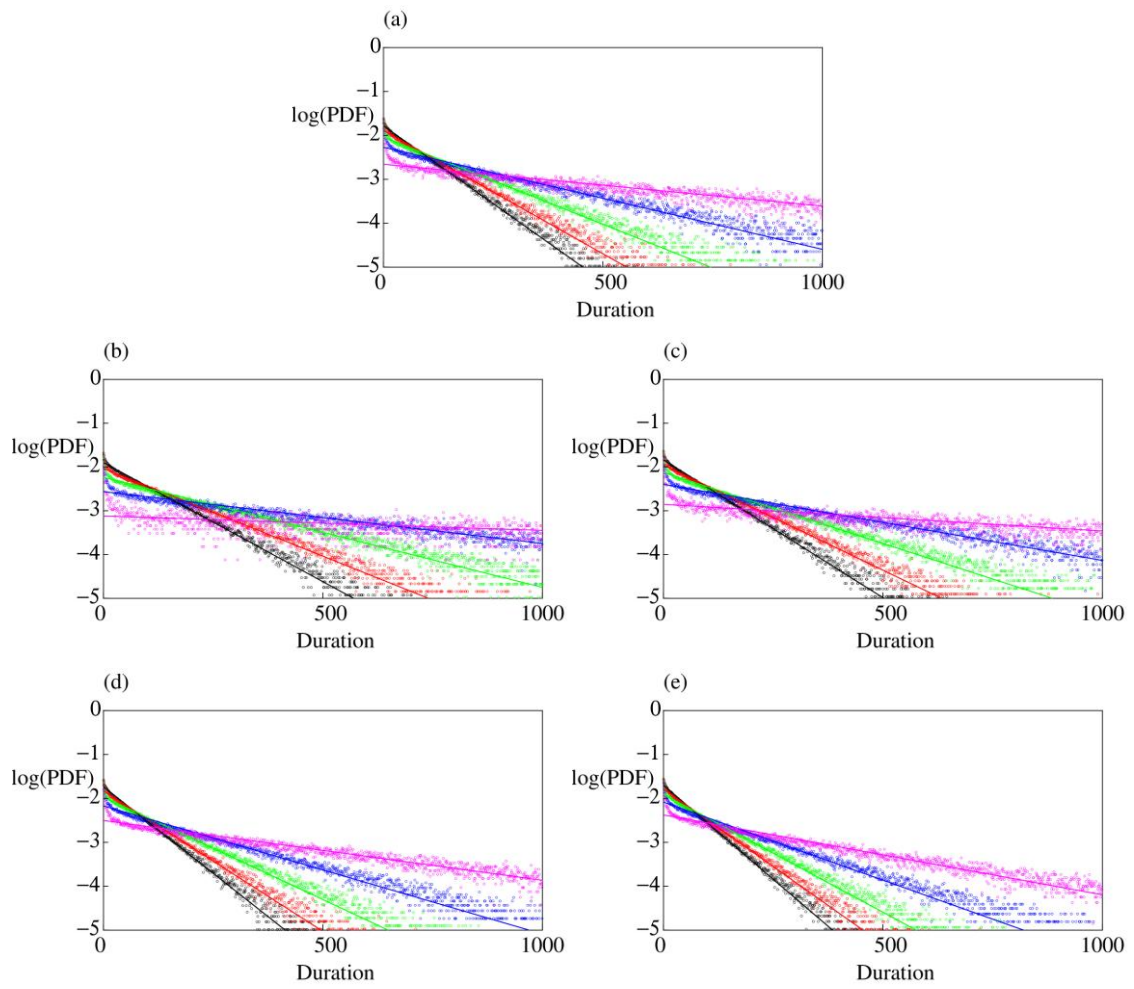


Figure 14. Comparison of the PDFs on the common logarithmic scale for durations of the low-flow periods, where circles and curves represent empirical and fitted results, respectively. The legends are the same as those in **Figure 13**.

Table 2. Average values of the streamflow discharge.

ε	Upper-bound case	Lower-bound case
0.159	22.8246	13.3516
0.631	28.6914	9.7366

Table 3 Average and variance of durations for high-flow periods computed by the benchmark and distorted model: $X_{thr} = 20$ (m³/s). “CV” means coefficient of variation.

ε	Benchmark	Upper-bound case		Lower-bound case	
	0	0.159	0.631	0.159	0.631
No. of samples	176425	189113	192732	159940	140026
Average (h)	2.198.E+01	2.470.E+01	2.942.E+01	1.913.E+01	1.669.E+01
Variance (h)	1.254.E+05	2.778.E+04	7.245.E+05	1.028.E+04	1.764.E+04
CV (-)	1.611.E+01	6.747.E+00	2.894.E+01	5.297.E+00	7.959.E+00

Table 4 Average and variance of durations for low-flow periods computed by the benchmark and distorted model: $X_{thr} = 20$ (m³/s).

ε	Benchmark	Upper-bound case		Lower-bound case	
	0	0.159	0.631	0.159	0.631
No. of samples	176425	189113	192733	159941	140026
Average (h)	7.725.E+01	6.788.E+01	6.143.E+01	9.033.E+01	1.083.E+02
Variance (h)	6.851.E+03	5.230.E+03	4.289.E+03	9.302.E+03	1.335.E+04
CV (-)	1.071.E+00	1.065.E+00	1.066.E+00	1.068.E+00	1.066.E+00

Table 5 Average and variance of durations for high-flow periods computed by the benchmark and distorted model: $X_{thr} = 160$ (m³/s).

ε	Benchmark	Upper-bound case		Lower-bound case	
	0	0.159	0.631	0.159	0.631
No. of samples	37742	53569	70613	24301	13217
Average (h)	7.280.E+00	7.953.E+00	9.083.E+00	5.784.E+00	4.426.E+00
Variance (h)	1.083.E+04	3.054.E+03	2.718.E+03	8.676.E+02	2.648.E+02
CV (-)	1.430.E+01	6.948.E+00	5.739.E+00	5.093.E+00	3.676.E+00

Table 6 Average and variance of durations for low-flow periods computed by the benchmark and distorted model: $X_{thr} = 160$ (m³/s).

ε	Benchmark	Upper-bound case		Lower-bound case	
	0	0.159	0.631	0.159	0.631
No. of samples	37742	53569	70613	24301	13217
Average (h)	4.565.E+02	3.188.E+02	2.388.E+02	7.144.E+02	1.320.E+03
Variance (h)	2.506.E+05	1.219.E+05	7.170.E+04	6.016.E+05	1.984.E+06
CV (-)	1.097.E+00	1.095.E+00	1.121.E+00	1.086.E+00	1.067.E+00

Table 7. Fitted values of the shape parameter ζ (-) and scaling parameter ϑ (h) for high-flow periods: $X_{\text{thr}} = 20 \text{ (m}^3/\text{s)}.$

ε	Benchmark	Upper-bound case		Lower-bound case	
	0	0.159	0.631	0.159	0.631
ζ (-)	2.004.E+00	2.022.E+00	2.001.E+00	2.036.E+00	2.016.E+00
ϑ (h)	2.207.E+01	2.525.E+01	2.945.E+01	1.982.E+01	1.695.E+01

Table 8. Fitted values of the shape parameter ζ (-) and scaling parameter ϑ (h) for high-flow periods: $X_{\text{thr}} = 160 \text{ (m}^3/\text{s)}.$

ε	Benchmark	Upper-bound case		Lower-bound case	
	0	0.159	0.631	0.159	0.631
ζ (-)	2.005.E+00	2.021.E+00	2.030.E+00	2.039.E+00	2.074.E+00
ϑ (h)	7.315.E+00	8.117.E+00	9.359.E+00	6.007.E+00	4.754.E+00

Table 9. Percentages of the occurrence of high-flow periods for different X_{thr} values.

ε	Benchmark	Upper-bound case		Lower-bound case	
	0	0.159	0.631	0.159	0.631
$X_{\text{thr}} = 20 \text{ (m}^3/\text{s)}$	22.14%	26.66%	32.36%	17.47%	13.34%
$X_{\text{thr}} = 160 \text{ (m}^3/\text{s)}$	1.57%	2.43%	3.66%	0.80%	0.33%

5. Conclusion

We proposed a novel mathematical framework for modeling uncertainties of long-memory processes based on the divergences on Musielak–Orlicz spaces that is suited to analyzing jump-driven supOU processes. Proper Musielak–Orlicz spaces were constructed on the basis of reversion and Lévy measures. We resolved the drawback of the classical KL divergence that fails to well-define cumulants subject to uncertainties by allowing for its state-dependence. We discussed the worst-case cumulants along with sufficient conditions for solvability of the corresponding optimization problems. The form of the worst-case cumulants enabled us to compute them by a gradient descent method with quantization. The application study demonstrated how uncertainties in reversion and Lévy measures affect the behavior of supOU processes, particularly their PDFs and threshold statistics. This paper suggested that distorted supOU processes based on Musielak–Orlicz spaces leads to a rigorous as well as computable approach for modeling uncertainties in long-memory phenomena.

A limitation of this study is that we only considered supOU processes, while there exist many other long-memory processes. Because the proposed mathematical framework for modeling uncertainties could simultaneously deal with distortions of multiple measures, it can be extended to many other jump-driven ambit and random fields driven by jump measures [76,77]. Another limitation of this study is the range of application areas of supOU processes because we only discussed environmental applications, while there would potentially exist a wide variety of problems described by jump-driven long-memory processes. In this view, a potential future research direction is to accumulate case studies of supOU and related processes in diverse research fields and integrate the uncertainty characteristics of each problem toward the development of a more versatile mathematical framework for modeling uncertainties in complex phenomena with long memory. Finally, because we could characterize uncertainties in the discharge data in view of Musielak–Orlicz spaces, an interesting future research topic would be mapping rivers and/or river systems via their associated Musielak–Orlicz spaces, so that we can better understand aquatic system dynamics from a different perspective than before.

Appendix

A1. Proofs

Proof of Proposition 1

The proof for the first part, except for stationarity, is by a direct adaptation of Proposition 39 in Barndorff-Nielsen et al. [21] combined with the assumption that in the present case there is no diffusion part, and the jumps are nonnegative. The stationarity follows from a direct calculation analogous to that of Proof of Theorem 3.1 in Barndorff-Nielsen [8]. The second part follows from the calculations analogous to Proof of Proposition 2.6 in Rajput and Rosinski [10].

□

Proof of Proposition 2

The proof relies on a Tauberian argument that connects the tail of an autocorrelation function and the singularity of the integrand (Proof of Proposition 6 in Fasen and Klüppelberg [51]) along with the assumption (10).

□

Proof of Proposition 3

First, we show the dual formulation (32) by following the lines of Proof of Proposition 3.19 in Fröhlich and Williamson [36]. The difference is that we are using Musielak–Orlicz spaces whereas the literature uses a classical Orlicz spaces.

The admissible set $\mathfrak{A}_{m,\varepsilon}$ is not a null set because the const function $\phi \equiv 1$ belongs to it, and hence, there exist Lagrangian multipliers $(\tau^*, \mu^*) \in [0, +\infty) \times \mathbb{R}$ such that (Proof of Theorem 5.1 in Dommel and Pichler [52])

$$\bar{I}_{k,m} = \frac{mc_m}{k} \sup_{\phi \geq 0} \left\{ \mathbb{E}_m [z^{k-m} \phi] - \tau^* \left(\mathbb{D}'(\phi) - \frac{\varepsilon}{mc_m} \right) - \mu^* (\mathbb{E}_m [\phi] - 1) \right\}, \quad (67)$$

and the nonnegativity as well as lower-semi continuity of Φ shows

$$\bar{I}_{k,m} = \frac{mc_m}{k} \inf_{\mu \in \mathbb{R}, \tau > 0} \sup_{\phi \geq 0} \left\{ \mathbb{E}_m [z^{k-m} \phi] - \tau \left(\mathbb{D}'(\phi) - \frac{\varepsilon}{mc_m} \right) - \mu (\mathbb{E}_m [\phi] - 1) \right\}, \quad (68)$$

where the supremum is taken with respect to nonnegative random variables on $(0, +\infty)^2$. We proceed as

$$\begin{aligned} \bar{I}_{k,m} &= \frac{mc_m}{k} \inf_{\mu \in \mathbb{R}, \tau > 0} \left\{ \frac{\varepsilon}{mc_m} \tau + \mu + \tau \sup_{\phi \geq 0} \left(\mathbb{E}_m \left[\frac{z^{k-m} - \mu}{\tau} \phi \right] - \mathbb{D}'(\phi) \right) \right\} \\ &= \frac{mc_m}{k} \inf_{\mu \in \mathbb{R}, \tau > 0} \left\{ \frac{\varepsilon}{mc_m} \tau + \mu + \tau \mathbb{E}_m \left[\Psi \left(w'(r, z), \alpha(r, z), \frac{z^{k-m} - \mu}{\tau} \right) \right] \right\} \\ &= \frac{mc_m}{k} \inf_{\mu \in \mathbb{R}, \tau > 0} \tau \left\{ \frac{\varepsilon}{mc_m} + \sigma + \mathbb{E}_m \left[\Psi \left(w'(r, z), \alpha(r, z), \frac{z^{k-m}}{\tau} - \sigma \right) \right] \right\}, \end{aligned} \quad (69)$$

where we applied the replacement $\mu = \tau\sigma \in \mathbb{R}$ to obtain the last line; the second line proves (32).

Second, we show that the infimum is attained at an interior point. This does not occur if and only if τ inside of the third line in (69) tends toward 0, where we used the functional similarity of the optimization problems between ours and that in the latter half of Proof of Proposition 5.5 in Dommel and Pichler [52]. If τ inside of the third line in (69) tends toward 0, then $\hat{\tau} = 0$ and hence

$$\begin{aligned}\bar{I}_{k,m} &= \sup_{\phi \geq 0} \left\{ \mathbb{E}_m \left[z^{k-m} \phi \right] - \hat{\tau} \left(\mathbb{D}'(\phi) - \frac{\varepsilon}{mc_m} \right) - \hat{\mu} (\mathbb{E}_m [\phi] - 1) \right\} \\ &= \sup_{\phi \geq 0} \left\{ \mathbb{E}_m \left[z^{k-m} \phi \right] - \hat{\mu} (\mathbb{E}_m [\phi] - 1) \right\} \\ &= +\infty,\end{aligned}\tag{70}$$

where the last line is due to **Assumption 2**, and we can realize it by considering ϕ that is concentrated at an arbitrary large $z > 0$ because $k > m$. However, we have the following upper bound of $\bar{I}_{k,m}$, leading to a contradiction:

$$\begin{aligned}\bar{I}_{k,m} &\leq \frac{mc_m}{k} \tau \left\{ \frac{\varepsilon}{mc_m} + \mu + \mathbb{E}_m \left[\Psi \left(w'(r, z), \alpha(r, z), \frac{z^{k-m} - \mu}{\tau} \right) \right] \right\} \Big|_{\tau=1, \mu=0} \\ &= \frac{mc_m}{k} \left\{ \frac{\varepsilon}{mc_m} + \mathbb{E}_m \left[\Psi \left(w'(r, z), \alpha(r, z), z^{k-m} \right) \right] \right\} \\ &\leq \frac{mc_m}{k} \left\{ \frac{\varepsilon}{mc_m} + \mathbb{E}_m \left[\bar{\Psi} \left(w'(r, z), \alpha(r, z), z^{k-m} \right) \right] \right\} \\ &< +\infty,\end{aligned}\tag{71}$$

where the last line is due to $z^{k-m} \in L_{\bar{\Psi}}$ and **Assumption 3**. Therefore, the infimum is attained at an interior point $(\hat{\tau}, \hat{\mu}) \in (0, +\infty) \times \mathbb{R}$, which is a minimizer. For the nonnegativity of $\hat{\mu}$, because the function $\bar{\Psi}(w_0, \alpha_0, y) - y$ ($y \in \mathbb{R}$) is nonnegative, nondecreasing, and convex for any $w_0 > 0$ and $\alpha_0 > 1$, the infimum for μ in the second line of (69) is not attained for $\mu < 0$; indeed, we have

$$\begin{aligned}\mu + \tau \mathbb{E}_m \left[\Psi \left(w', \alpha, \frac{z^{k-m} - \mu}{\tau} \right) \right] &= \tau \left(\mathbb{E}_m \left[\Psi \left(w', \alpha, \frac{z^{k-m}}{\tau} - \frac{\mu}{\tau} \right) \right] - \mathbb{E}_m \left[\frac{z^{k-m}}{\tau} - \frac{\mu}{\tau} \right] \right) + \mathbb{E}_m [z^{k-m}] \\ &(\equiv \tau H_\tau(\mu) + \mathbb{E}_m [z^{k-m}])\end{aligned}\tag{72}$$

for all $\tau > 0$, $H_\tau(0)$ is finite, and $H_\tau(\mu)$ is nonincreasing for $\mu \geq 0$.

The maximizer ϕ^* of the optimization problem is obtained as a byproduct of (69). Indeed, it satisfies

$$\frac{z^{k-m} - \hat{\mu}}{\hat{\tau}} = \frac{\partial \Phi}{\partial \phi} (w', \alpha, \phi^*) \text{ for } (r, z) \text{ such that } \phi^* > 0,\tag{73}$$

and hence $\phi^*(r, z)$ is given by (33) because $\frac{\partial \Phi}{\partial \phi}(\cdot, \cdot, \phi)$ is the inverse of $\frac{\partial \Psi}{\partial \psi}(\cdot, \cdot, \psi)$ (with respect to the third argument), and hence

$$\frac{\partial \Psi}{\partial \psi} \left(w', \alpha, \frac{z^{k-m} - \hat{\mu}}{\hat{\tau}} \right) = \frac{\partial \Psi}{\partial \psi} \left(w', \alpha, \frac{\partial \Phi}{\partial \phi} (w', \alpha, \phi^*) \right) = \phi^*. \quad (74)$$

The fact that the couple $(\hat{\tau}, \hat{\mu})$ solves (34) is due to the continuous differentiability of F .

Finally, we show that the condition (\mathbf{I}_k) with ϕ^* holds true. The assumption $z^{k-m} \in L_{\bar{\Psi}}$ leads to the fact that the optimizer ϕ^* given in (33) satisfies the condition $\mathbb{D}'(\phi^*) < +\infty$ due to its definition, and hence, $\phi^* \in L_{\bar{\Phi}}$. This implies that the condition (\mathbf{I}_k) with ϕ^* holds true because, by the Fenchel–Yoshioka inequality between $\bar{\Phi}$ and $\bar{\Psi}$ (Lemma 2.1.32 in Chlebicka et al. [33]), we obtain

$$\begin{aligned} & \int_{r=0}^{r=+\infty} \int_{z=0}^{z=+\infty} \phi(r, z) z^{k-m} p_m(dr, dz) \\ & \leq \int_{r=0}^{r=+\infty} \int_{z=0}^{z=+\infty} \bar{\Phi}(w', \alpha, \phi^*(r, z)) p_m(dr, dz) + \int_{r=0}^{r=+\infty} \int_{z=0}^{z=+\infty} \bar{\Psi}(w', \alpha, z^{k-m}) p_m(dr, dz) \\ & < +\infty, \end{aligned} \quad (75)$$

where the last line comes from $\phi^* \in L_{\bar{\Phi}}$ and $z^{k-m} \in L_{\bar{\Psi}}$ along with **Assumption 3**. □

Proof of Proposition 4

Most parts of the proof here are the same as those for **Proposition 3** except for the point to prove $\hat{\mu} \in (-\infty, 0]$. This is due to $0 \leq \frac{\partial \Psi}{\partial \psi}(w_0, \alpha_0, \psi) \leq 1$ for any $w_0 > 0$, $\alpha_0 > 1$, and $\psi \leq 0$. Indeed, because we need $\mathbb{E}_m[\phi^*] = 1$, $\hat{\mu}$ must be positive considering the representation (37) and $-\frac{z^{k-m}}{\hat{\tau}} \leq 0$; otherwise, we face $\phi^* < 1$ and the condition $\mathbb{E}_m[\phi^*] = 1$ is never satisfied. □

Proof of Proposition 5

By **Definition 1**, if $\phi \in L_{\bar{\Phi}(w'_2, \alpha_2, \cdot)}$ then $\phi \in L_{\bar{\Phi}(w'_1, \alpha_1, \cdot)}$, and therefore the first part of the proof holds true.

The second part is due to the following inequality: for $\phi \in L_{\bar{\Phi}(w'_2, \alpha_2, \cdot)}$,

$$\|\phi\|_{(w'_2, \alpha_2, \cdot)} = \inf \left\{ c > 0 \mid \mathbb{E}_m \left[\bar{\Phi} \left(w'_2, \alpha_2, \frac{|\phi|}{c} \right) \right] \leq 1 \right\} \geq \inf \left\{ c \mathbb{E}_m \left[\bar{\Phi} \left(w'_1, \alpha_1, \frac{|\phi|}{c} \right) \right] \leq 1 \right\} = \|\phi\|_{(w'_1, \alpha_1, \cdot)}. \quad (76)$$

□

A2. Numerical method

We apply the following gradient descent with momentum to solve the system (34), which is a version of the Nesterov method (e.g., Walkington [78]):

$$\begin{aligned}\lambda_{n+1} &= \omega\lambda_n - \eta_n \frac{\partial F(\tau_n + \omega\lambda_n, \mu_n + \omega\rho_n)}{\partial \tau}, \quad n=0,1,2,\dots \\ \tau_{n+1} &= \tau_n + \lambda_n\end{aligned}\tag{77}$$

and

$$\begin{aligned}\rho_{n+1} &= \omega\rho_n - \kappa_n \frac{\partial F(\tau_n + \omega\lambda_n, \mu_n + \omega\rho_n)}{\partial \mu}, \quad n=0,1,2,\dots \\ \mu_{n+1} &= \mu_n + \rho_n\end{aligned}\tag{78}$$

with an initial guess $(\tau_0, \mu_0) \in (0, +\infty) \times \mathbb{R}$ and $(\lambda_0, \rho_0) \in \mathbb{R}^2$. Here, the subscript n represents the time step, $\omega (=0.95)$ is a relaxation factor, λ is momentum for numerical τ , ρ is momentum for numerical μ , and η and κ are learning rates for τ and μ , respectively. The partial derivatives are discretized by using the quantization method (58). The recursions (77) and (78) are terminated if

$$\left| \frac{\partial F(\tau_n + \omega\lambda_n, \mu_n + \omega\rho_n)}{\partial \mu} \right|, \left| \frac{\partial F(\tau_n + \omega\lambda_n, \mu_n + \omega\rho_n)}{\partial \tau} \right| \leq \delta,\tag{79}$$

where $\delta > 0$ is a prescribed error threshold and (τ_{n+1}, μ_{n+1}) is considered an approximation of $(\hat{\tau}, \hat{\mu})$.

We empirically found that the following learning rates work well for our computational case:

$$\eta_n = 2.5\varepsilon^{-1} \quad \text{and} \quad \kappa_n = 0.25\tau_n^{-1}\tag{80}$$

based on the preliminary finding that τ_n is large, such as $O(10^2)$ or larger, and a small η_n is needed for the stability of the algorithm when ε is large.

Here, we report the computational costs of the proposed numerical algorithm, where we set $M = 512$. **Tables A1-A2** show the iteration count and computed $(\hat{\tau}, \hat{\mu})$ for different values of ε for $\alpha \equiv 2.5, 4.0, 5.0$. Here, for each α , we start the computation from $\varepsilon = 10^{2-0.6 \times 0}$ and the initial guess at $\varepsilon = 10^{2-0.6 \times 1}$ is that of the numerical solution at $\varepsilon = 10^{2-0.6 \times 0}$. This procedure is iterated for subsequent computations for $\varepsilon = 10^{2-0.6i}$ ($i = 2, 3, \dots$). The initial guess at $\varepsilon = 10^{2-0.6 \times 0}$ is $(\tau, \mu) = (500, 100)$ for both **Upper- and Lower-bound cases**. The iteration count needed to obtain a numerical solution increases as ε decreases under the present computational setting, where we should use a large learning parameter due to a small $\hat{\tau}$, as indicated in **Section 3.3**. This implies the need for a larger number of iterations with (sufficiently small) constant η and κ values. The iteration counts among different α values are not critically different, and the computational costs for **Upper- and Lower-bound cases** are comparable. **Table A3** compares the exact and computed variances for different values of M . The relative error at $M = 512$ used in the main text is 0.056%, and the convergence order of the discretization is approximately 1; the relative error behaves as $O(M^{-1})$ because the error is almost halved by doubling M .

Table A1. Iteration counts for convergence: **Upper-bound case.**

i	ε	$\alpha \equiv 2.5$	$\alpha \equiv 4.0$	$\alpha \equiv 5.0$
0	1.000.E+02	727	611	621
1	2.512.E+01	632	548	517
2	6.310.E+00	1092	569	573
3	1.585.E+00	1738	1467	1263
4	3.981.E-01	3918	3378	3154
5	1.000.E-01	8226	7645	7242
6	2.512.E-02	16660	16435	15917
7	6.310.E-03	32912	34033	33628
8	1.585.E-03	63803	68329	68640
9	3.981.E-04	121944	133869	136151
10	1.000.E-04	230607	257622	264250

Table A2. Iteration counts for convergence: **Lower-bound case.**

i	ε	$\alpha \equiv 2.5$	$\alpha \equiv 4.0$	$\alpha \equiv 5.0$
0	1.000.E+02	539	522	519
1	2.512.E+01	501	501	501
2	6.310.E+00	521	501	501
3	1.585.E+00	1004	950	944
4	3.981.E-01	3570	3427	3301
5	1.000.E-01	9445	10003	9832
6	2.512.E-02	20910	22434	25415
7	6.310.E-03	38327	29104	13366
8	1.585.E-03	68744	82046	97235
9	3.981.E-04	126670	106563	181052
10	1.000.E-04	235436	267078	273483

Table A3. Maximum errors between exact and computed variances. The exact variance is 1472.48 (m^6/s^2).

Resolution M	Computed variance (m^6/s^2)	Relative error (%)
32	1459.32	0.894
64	1465.89	0.448
128	1469.19	0.223
256	1470.83	0.112
512	1471.66	0.056

A3. Influences of regularization

Figure A1 shows the computed variance values of the distorted supOU processes for different values of ε in **Upper- and Lower-bound cases** with different regularization parameter W values, demonstrating that the regularization does not quantitatively affect the variance values under uncertainties. **Figures A2-A3** show the computed ϕ^* for different W values with $\alpha \equiv 4.0$ and $\varepsilon = 6.31$ in **Upper- and Lower-bound cases**, respectively. Weakening the regularization by choosing a larger value of W results in a more heterogeneous ϕ^* , but its influences seem to be less significant in the **Lower-bound case**. The examined W values do not affect qualitative profiles of ϕ^* for the computational cases examined here. We empirically found that specifying a weaker regularization (i.e., larger W value) results in slower convergence or nonconvergence of the computational method, which is due to the coexistence of terms ranging across more than several tens of orders in the summation (58). The regularization therefore avoids this computational failure. Development of a stable computational methodology to deal with integrands without regularizations is currently undergoing.

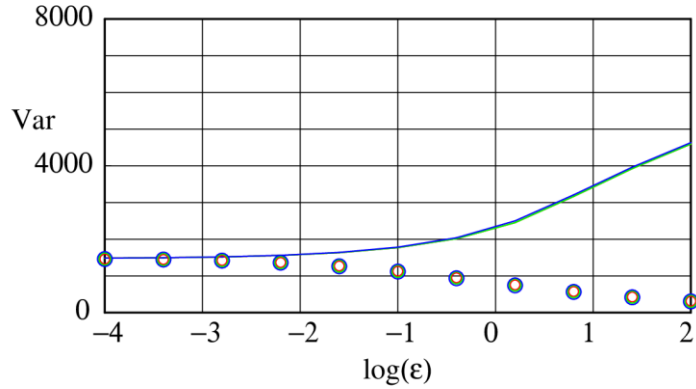


Figure A1. Computed variance (Var) (m^6/s^2) values of the distorted supOU processes in **Upper-bound case** (curves) and **Lower-bound case** (circles) with different regularization parameter W (h) values: $W = 0.1$ (red), $W = 1$ (green), and $W = 10$ (blue).

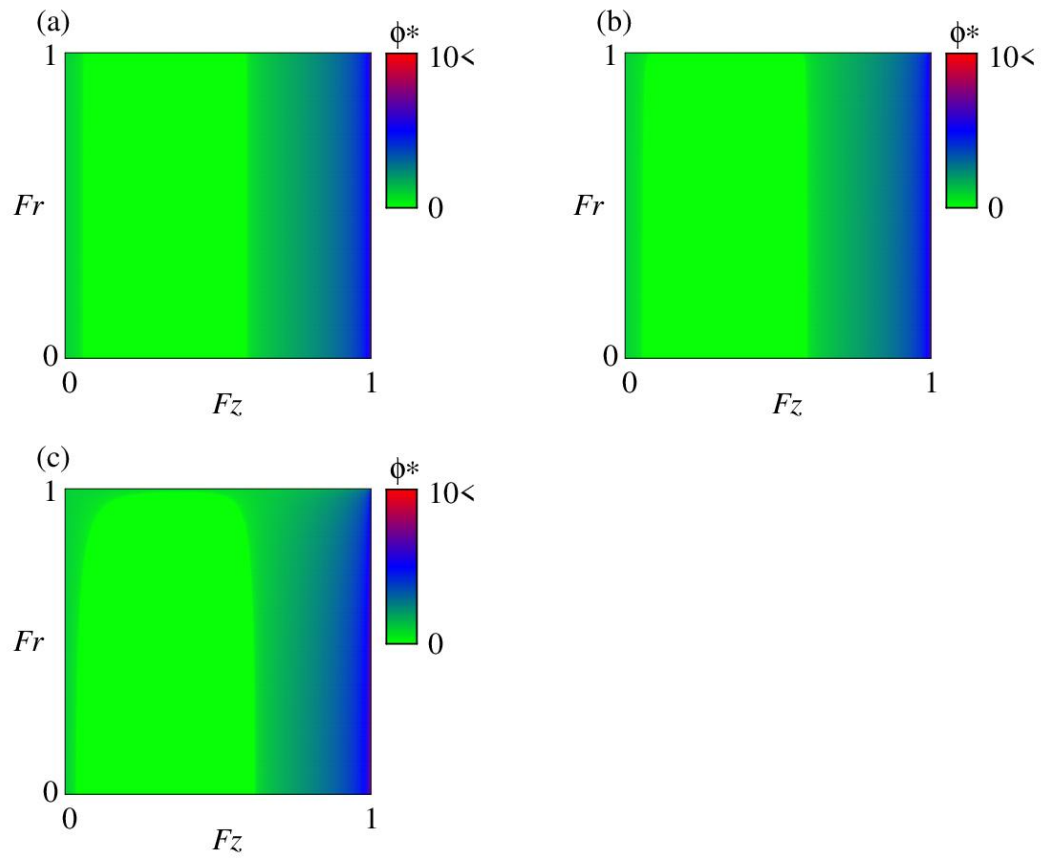


Figure A2. Computed ϕ^* for different W (h) values with $\alpha \equiv 4.0$ and $\varepsilon = 6.31$ in **Upper-bound case**: (a) $W = 0.1$, (b) $W = 1$, (c) $W = 10$.

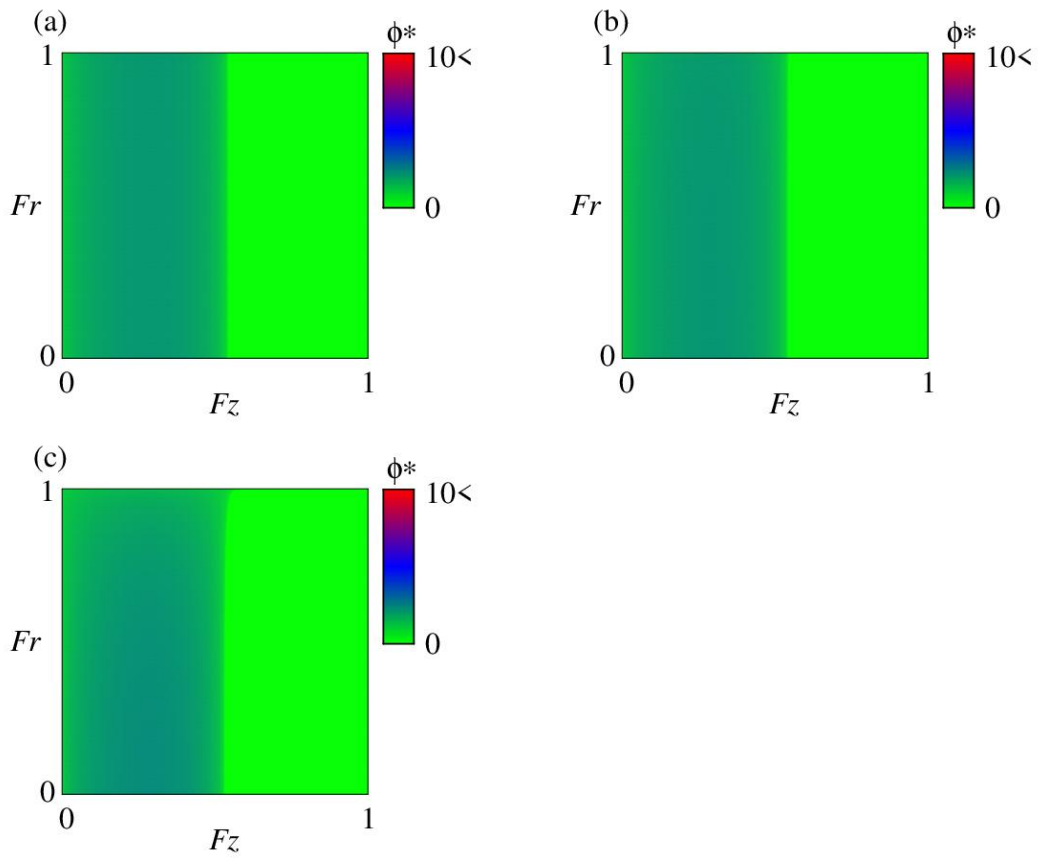


Figure A3. Computed ϕ^* for different W (h) values with $\alpha \equiv 4.0$ and $\varepsilon = 6.31$ in **Lower-bound case**: (a) $W = 0.1$, (b) $W = 1$, (c) $W = 10$.

References

- [1] Beran, J., Feng, Y., Ghosh, S., Kulik, R. (2013). Long-Memory Processes. Springer, Berlin, Heidelberg.
- [2] Lanoiselée, Y., Pagnini, G., & Wyłomańska, A. (2025). Super-resolved anomalous diffusion: deciphering the joint distribution of anomalous exponent and diffusion coefficient. *Physical Review Letters*, 135(13), 137101. <https://doi.org/10.1103/PhysRevLett.135.137101>
- [3] Montes, R. M., & Quinones, R. A. (2025). Early detection of sea lice epidemic transitions and changes in long-term abundance levels in salmon farming areas. *Aquaculture*, 603, 742385. <https://doi.org/10.1016/j.aquaculture.2025.742385>
- [4] Zhao, X., & Hou, W. Intelligent parameter identification for the Black-Scholes system driven by mixed fractional Brownian motion. *Chaos, Solitons & Fractals*, 207, 118022. <https://doi.org/10.1016/j.chaos.2026.118022>
- [5] Laskin, N. (2024). A new approach to constructing probability distributions of fractional counting processes. *Chaos, Solitons & Fractals*, 186, 115268. <https://doi.org/10.1016/j.chaos.2024.115268>
- [6] Balagula, Y., Baimel, D., & Aharon, I. (2025). Comparing time series and neural network models of long memory for electricity price forecasting. *Results in Engineering*, 108465. <https://doi.org/10.1016/j.rineng.2025.108465>
- [7] Elnady, S. M., El-Beltagy, M., Radwan, A. G., & Fouda, M. E. (2025). A comprehensive survey of fractional gradient descent methods and their convergence analysis. *Chaos, Solitons & Fractals*, 194, 116154. <https://doi.org/10.1016/j.chaos.2025.116154>
- [8] Barndorff-Nielsen, O. E. (2001). Superposition of Ornstein–Uhlenbeck type processes. *Theory of Probability & Its Applications*, 45(2), 175-194. <https://doi.org/10.1137/S0040585X97978166>
- [9] Barndorff-Nielsen, O. E., & Stelzer, R. (2011). Multivariate supOU processes. <https://doi.org/10.1214/10-AAP690>
- [10] Rajput, B. S., & Rosinski, J. (1989). Spectral representations of infinitely divisible processes. *Probability Theory and Related Fields*, 82(3), 451-487. <https://doi.org/10.1007/BF00339998>
- [11] Chen, W., & Huang, S. (2025). A novel detection approach of bifurcation-induced tipping points with generalized Ornstein-Uhlenbeck process in finance. *Chaos, Solitons & Fractals*, 201, 117257. <https://doi.org/10.1016/j.chaos.2025.117257>
- [12] Gu, A., He, X., Chen, S., & Yao, H. (2023). Optimal investment-consumption and life insurance strategy with mispricing and model ambiguity. *Methodology and Computing in Applied Probability*, 25(3), 77. <https://doi.org/10.1007/s11009-023-10051-0>
- [13] Kabanov, Y., & Sonin, M. A. (2025). On the entropy-minimal martingale measure in the exponential Ornstein–Uhlenbeck stochastic volatility model. *Annals of Operations Research*. Published online. <https://doi.org/10.1007/s10479-025-06941-w>
- [14] Barndorff-Nielsen, O. E., & Stelzer, R. (2013). The multivariate supOU stochastic volatility model. *Mathematical Finance: An International Journal of Mathematics, Statistics and Financial Economics*, 23(2), 275-296. <https://doi.org/10.1111/j.1467-9965.2011.00494.x>
- [15] Yoshioka, H. (2021). Fitting a superposition of Ornstein–Uhlenbeck process to time series of discharge in a perennial river environment. *The Proceedings of ANZIAM*, 63, C84-C96. <https://doi.org/10.21914/anziamj.v63.16985>
- [16] Yoshioka, H. (2025). Superposition of interacting stochastic processes with memory and its application to migrating fish counts. *Chaos, Solitons & Fractals*, 192, 115911. <https://doi.org/10.1016/j.chaos.2024.115911>
- [17] Kovtun, A., Leonenko, N., & Pepelyshev, A. (2025). Singular properties of high-order spectral densities of supOU processes. *Communications in Nonlinear Science and Numerical Simulation*, 109459. <https://doi.org/10.1016/j.cnsns.2025.109459>
- [18] Grahovac, D., & Kevei, P. (2025). Tail behavior and almost sure growth rate of superpositions of Ornstein–Uhlenbeck-type processes. *Journal of theoretical probability*, 38(1), 1. <https://doi.org/10.1007/s10959-024-01374-w>
- [19] Moser, M., & Stelzer, R. (2011). Tail behavior of multivariate Lévy-driven mixed moving average processes and supOU stochastic volatility models. *Advances in Applied Probability*, 43(4), 1109-1135. <https://doi.org/10.1239/aap/1324045701>
- [20] Leonenko, N. N., & Pepelyshev, A. (2026). Simulation of supOU processes with specified marginal distribution and correlation function. *Modern Stochastics: Theory and Applications*. Published online. <https://doi.org/10.15559/25-VMSTA291>
- [21] Barndorff-Nielsen, O.E., Benth, F.E., & Veraart, A.E.D. (2018). *Ambit Stochastics*. Springer, Cham.
- [22] Behme, A., Chong, C., & Klüppelberg, C. (2015). Superposition of COGARCH processes. *Stochastic Processes and their Applications*, 125(4), 1426-1469. <https://doi.org/10.1016/j.spa.2014.11.004>
- [23] Yoshioka, H. (2026). Theoretical and computational investigations of superposed interacting affine and more complex processes. *Mathematics and Computers in Simulation*, 245, 628-654. <https://doi.org/10.1016/j.matecom.2026.01.013>
- [24] Luo, H., Yang, Q., Mazloff, M., Neger, L., & Chen, D. (2023). The impacts of optimizing model-dependent parameters on the Antarctic sea ice data assimilation. *Geophysical Research Letters*, 50(22), e2023GL105690. <https://doi.org/10.1029/2023GL105690>
- [25] Shao, Y., & Si, W. (2021). Degradation modeling with long-term memory considering measurement errors. *IEEE Transactions on Reliability*, 72(1), 177-189. <https://doi.org/10.1109/TR.2021.3125958>
- [26] Liu, N., Qian, L., Yan, D., Hu, W., & Hong, M. (2024). A nonlinear dynamical model for monthly runoff forecasting in situations of small samples. *Mathematical Geosciences*, 56(3), 639-659. <https://doi.org/10.1007/s11004-023-10099-1>
- [27] Ma, C., & Yuan, N. (2025). Exploring land surface air temperature changes: a detailed trend analysis through the lens of long-term memory. *Climate Dynamics*, 63(8), 295. <https://doi.org/10.1007/s00382-025-07791-9>
- [28] Dyson, M., & Stemler, T. (2025). Improving forecasts of imperfect models using piecewise stochastic processes. *Chaos: An Interdisciplinary Journal of Nonlinear Science*, 35(2). <https://doi.org/10.1063/5.0242061>
- [29] Hansen, L. P., & Souttou, P. (2025). Stochastic responses and marginal valuation. *Proceedings of the National Academy of Sciences*, 122(48), e2520857122. <https://doi.org/10.1073/pnas.2520857122>
- [30] Yoshioka, H., & Yoshioka, Y. (2024). Generalized divergences for statistical evaluation of uncertainty in long-memory processes. *Chaos, Solitons & Fractals*, 182, 114627. <https://doi.org/10.1016/j.chaos.2024.114627>
- [31] Yoshioka, H., Tomobe, H., & Yoshioka, Y. (2024). Orlicz risks for assessing stochastic streamflow environments: a static optimization approach. *Stochastic Environmental Research and Risk Assessment*, 38(1), 233-250. <https://doi.org/10.1007/s00477-023-02561-7>
- [32] Strati, F. (2025). Risk measures on Musielak-Orlicz spaces: A state-dependent perspective for insurance. *Insurance: Mathematics and Economics*, 103174. <https://doi.org/10.1016/j.insmatheco.2025.103174>
- [33] Chlebicka, I., Gwiazda, P., Āwierczewska-Gwiazda, A., Wróblewska-Kamińska, A. (2021). *Partial Differential Equations in Anisotropic Musielak-Orlicz*. Springer, Cham.
- [34] Sason, I., & Verdú, S. (2016). f -divergence Inequalities. *IEEE Transactions on Information Theory*, 62(11), 5973-6006. <https://doi.org/10.1109/TIT.2016.2603151>

- [35] Ben-Tal, A., & Teboulle, M. (2007). An old-new concept of convex risk measures: the optimized certainty equivalent. *Mathematical Finance*, 17(3), 449-476. <https://doi.org/10.1111/j.1467-9965.2007.00311.x>
- [36] Fröhlich, C., & Williamson, R. C. (2023). Tailoring to the tails: Risk measures for fine-grained tail sensitivity. *Transactions on Machine Learning Research*. <https://openreview.net/pdf?id=UntUoeLwwu>
- [37] Rubshtein, B.Z. A., Grabarnik, G. Y., & Muratov, M. A., Pashkova, Y.S. (2016). *Foundations of Symmetric Spaces of Measurable Functions*. Developments in Mathematics. Springer, Cham.
- [38] Bellini, F., Laeven, R. J., & Rosazza Gianin, E. (2018). Robust return risk measures. *Mathematics and Financial Economics*, 12(1), 5-32. <https://doi.org/10.1007/s11579-017-0188-x>
- [39] Bellini, F., Laeven, R. J., & Gianin, E. R. (2021). Dynamic robust Orlicz premia and Haezendonck–Goovaerts risk measures. *European Journal of Operational Research*, 291(2), 438-446. <https://doi.org/10.1016/j.ejor.2019.08.049>
- [40] Chudziak, J., & Rela, P. (2025a). The Orlicz premium principle under uncertainty. *Revista de la Real Academia de Ciencias Exactas, Físicas y Naturales. Serie A. Matemáticas*, 119(4), 116. <https://doi.org/10.1007/s13398-025-01778-1>
- [41] Chudziak, J., & Rela, P. (2025b). On supertranslativity of the Orlicz premium principle. *Aequationes mathematicae*, 99(6), 2549-2563. <https://doi.org/10.1007/s00010-025-01207-z>
- [42] Ito, K., & Kashima, K. (2024). Risk-sensitive control as inference with Rényi divergence. *Advances in Neural Information Processing Systems*, 37, 71381-71413. <https://proceedings.neurips.cc/paper/2024/file/836cf992a71f7a0bda218c180f942902-Paper-Conference.pdf>
- [43] Póczos, B., & Schneider, J. (2011). On the Estimation of α -Divergences. In *Proceedings of the Fourteenth International Conference on Artificial Intelligence and Statistics*, pp. 609-617. JMLR Workshop and Conference Proceedings. <https://proceedings.mlr.press/v15/poczos11a/poczos11a.pdf>
- [44] Boyd, S., & Vandenberghe, L. (2004). *Convex optimization*. Cambridge University Press.
- [45] Chen, B., Chen, X., Zhang, Z., & Sun, H. (2025). Derivation and analysis of spatial variability in master recession curves with mixed effects model. *Journal of Hydrology*, 662, 133853. <https://doi.org/10.1016/j.jhydrol.2025.133853>
- [46] Gao, M., Wang, Z., Chen, X., Dong, J., & Singh, S. K. (2026). The key drivers of streamflow recession variability and their implications for robust parameterization of recession processes. *Hydrological Sciences Journal*. Published Online. <https://doi.org/10.1080/02626667.2025.2593328>
- [47] Zhang, R., Bu, Q., Chen, X., & Liu, J. (2025). Can storage-discharge characteristics of karst matrix system quantified through recession analysis be reliable?. *Journal of Hydrology*, 648, 132378. <https://doi.org/10.1016/j.jhydrol.2024.132378>
- [48] Boros, D., Borbás, E., Darougi, A., Kovács, J., & Márkus, L. (2025). A Fractional Process with Jumps for Modeling Karstic Spring Discharge Data. *Mathematics*, 13(18), 2928. <https://doi.org/10.3390/math13182928>
- [49] Devò, P., Basso, S., & Marani, M. (2025). Estimation of extreme floods using a statistical and conceptual model of the hydrological response. *Water Resources Research*, 61(5), e2024WR038667. <https://doi.org/10.1029/2024WR038667>
- [50] Houénafa, S. E., Ronoh, E. K., Johnson, O., & Moore, S. E. (2025). Lévy-induced stochastic differential equation models in rainfall-runoff systems for assessing extreme hydrological event risks. *Stochastic Environmental Research and Risk Assessment*, 39(4), 1537-1554. <https://doi.org/10.1007/s00477-025-02931-3>
- [51] Fasen, V., & Klüppelberg, C. (2007). Extremes of supOU processes. In *Stochastic analysis and applications: The Abel Symposium 2005*, pp. 339-359. Springer, Berlin, Heidelberg. https://doi.org/10.1007/978-3-540-70847-6_14
- [52] Dommel, P., & Pichler, A. (2021). Convex risk measures based on divergence. *Pure and Applied Functional Analysis*, 6(6), 1157-1181. <http://yokohamapublishers.jp/online2/oppafa/vol6/p1157.html>
- [53] Grabchak, M., & Saba, S. (2025). On approximations of subordinators in L^p and the simulation of tempered stable distributions. *Statistics and Computing*, 35(3), 54. <https://doi.org/10.1007/s11222-025-10586-x>
- [54] Zhu, Y., & Wang, L. (2026). Dynamics of a stochastic SIS model driven by Markovian switching and Lévy jump with heavy tailed increments. *Chaos, Solitons & Fractals*, 202, 117552. <https://doi.org/10.1016/j.chaos.2025.117552>
- [55] Chewi, S. (2025). *Lectures on Optimization*. Version May 6, 2025. https://chewisinho.github.io/opt_notes_final.pdf
- [56] Diakonikolas, J., & Jordan, M. I. (2021). Generalized momentum-based methods: A Hamiltonian perspective. *SIAM Journal on Optimization*, 31(1), 915-944. <https://doi.org/10.1137/20M1322716>
- [57] Xie, Z., Yin, W., & Wen, Z. (2025). ODE-Based Learning to Optimize: Z. Xie et al. *Mathematical Programming*. Published online. <https://doi.org/10.1007/s10107-025-02303-3>
- [58] Yoshioka, H. (2024). Modeling stationary, periodic, and long memory processes by superposed jump-driven processes. *Chaos, Solitons & Fractals*, 188, 115357. <https://doi.org/10.1016/j.chaos.2024.115357>
- [59] Al Sawaf, M. B., Kawanisi, K., Kagami, J., Bahreinimotlagh, M., & Dania, M. M. (2017). Scaling characteristics of mountainous river flow fluctuations determined using a shallow-water acoustic tomography system. *Physica A: Statistical Mechanics and its Applications*, 484, 11-20. <https://doi.org/10.1016/j.physa.2017.04.168>
- [60] Al Sawaf, M. B., & Kawanisi, K. (2020). Assessment of mountain river streamflow patterns and flood events using information and complexity measures. *Journal of Hydrology*, 590, 125508. <https://doi.org/10.1016/j.jhydrol.2020.125508>
- [61] Labat, D., Masbou, J., Beaulieu, E., & Mangin, A. (2011). Scaling behavior of the fluctuations in stream flow at the outlet of karstic watersheds, France. *Journal of hydrology*, 410(3-4), 162-168. <https://doi.org/10.1016/j.jhydrol.2011.09.010>
- [62] Lombardo, L., Papalexiou, S. M., Thébaud, C., Clark, M. P., Vogel, R. M., & Viglione, A. (2025). Residual dynamics in hydrological models: insights from a large sample of catchments and models. *Advances in Water Resources*, 105165. <https://doi.org/10.1016/j.advwatres.2025.105165>
- [63] McEachran, Z., Ghosh, R., Renganathan, A., Sharma, S., Lindsay, K., Steinbach, M., ... & Kumar, V. (2025). Knowledge-guided machine learning for operational flood forecasting. *Water Resources Research*, 61(11), e2024WR039064. <https://doi.org/10.1029/2024WR039064>
- [64] Iwata, K., & Sugita, S. (1990). The distribution of Dezukuri in Myoudani District. *Ishikawa Prefecture Hakusan Nature Conservation Center Research Report*, 17, 61-64. <https://www.pref.ishikawa.lg.jp/hakusan/publish/report/documents/report17-6.pdf> (in Japanese with English Abstract).
- [65] Tanaka, T., Kobayashi, K., & Tachikawa, Y. (2021). Simultaneous flood risk analysis and its future change among all the 109 class-A river basins in Japan using a large ensemble climate simulation database d4PDF. *Environmental Research Letters*, 16(7), 074059. <https://doi.org/10.1088/1748-9326/abfb2b>
- [66] Chen, J., Sayama, T., Yamada, M., Tanaka, T., & Sugawara, Y. (2025). Projecting multiscale river flood changes across Japan at +2 C and +4 C climates. *Earth's Future*, 13(5), e2024EF005884. <https://doi.org/10.1029/2024EF005884>

- [67] Abiko, K., & Taniguchi, K. (2026). Runoff analysis in the upper Tadori River basin considering changes in rainfall and snowfall under global warming. *Japanese Journal of JSCE*, 82(16), 25-16130. <https://doi.org/10.2208/jscej.25-16130> (in Japanese with English Abstract).
- [68] Yoshioka, H., & Yoshioka, Y. (2025). Non-Markovian superposition process model for stochastically describing concentration–discharge relationship. *Chaos, Solitons & Fractals*, 199, 116715. <https://doi.org/10.1016/j.chaos.2025.116715>
- [69] Chyon, M. S. A., Best, J., & Haq, S. M. A. (2026). From extraction to recovery: Geomorphic and social transformations of gravel mining, Lubha River, Northeast Bangladesh. *Cell Reports Sustainability*, 3(1). <https://doi.org/10.1016/j.crsus.2025.100605>
- [70] Le Guern, J., Jugé, P., Latosinski, F. G., Andréault, A., Wintemberger, C. L., & Rodrigues, S. (2026). Scaling up bedload monitoring: a passive acoustic approach for large river systems. *Science of the Total Environment*, 1013, 181330. <https://doi.org/10.1016/j.scitotenv.2025.181330>
- [71] Calvani, G., Carbonari, C., & Solari, L. (2022). Stability analysis of submerged vegetation patterns in rivers. *Water Resources Research*, 58(8), e2021WR031901. <https://doi.org/10.1029/2021WR031901>
- [72] Latella, M., Notti, D., Baldo, M., Giordan, D., & Camporeale, C. (2024). Short-term biogeomorphology of a gravel-bed river: Integrating remote sensing with hydraulic modelling and field analysis. *Earth Surface Processes and Landforms*, 49(3), 1156-1178. <https://doi.org/10.1002/esp.5760>
- [73] Nakamura, T., Maruyama, T., & Watanabe, S. (2001). Population Increase of the Fluvial Japanese Charr *Salvelinus leucomaenis* after Fishing Prohibition. *Nippon Suisan Gakkaishi*, 67(1), 105-107. <https://doi.org/10.2331/suisan.67.105> (in Japanese).
- [74] Huang, J., Shao, H., Gao, F., Song, J., & He, G. (2025). A data-driven prediction-decision framework for improving the resilience of hydropower systems under drought disasters. *Annals of Operations Research*. Published online. <https://doi.org/10.1007/s10479-025-06962-5>
- [75] Yoshioka, H., Yoshioka, Y., & Tsujimura, M. (2025). Tractable fish growth models considering individual differences with an application to the fish *Plecoglossus altivelis*. *Applied Mathematical Modelling*, 148, 116217. <https://doi.org/10.1016/j.apm.2025.116217>
- [76] Benth, F. E., & Veraart, A. E. (2026). Research frontiers in ambit stochastics: In memory of Ole E. Barndorff-Nielsen. *Bernoulli*, 32(1), 24-48. <https://doi.org/10.3150/25-BEJ1902>
- [77] Donhauzer, I., Leonenko, N., & Olenko, A. (2025). Construction and limit theorems for supCAR fields. Preprint, arXiv:2505.21195. <https://doi.org/10.48550/arXiv.2505.21195>
- [78] Walkington, N. J. (2023). Nesterov's method for convex optimization. *SIAM Review*, 65(2), 539-562. <https://doi.org/10.1137/21M1390037>